Published by
NIGERIAN SOCIETY OF PHYSICAL SCIENCES
Available online @ https://journal.nsps.org.ng/index.php/jnsps

J. Nig. Soc. Phys. Sci. 8 (2026) 3539

Journal of the Nigerian Society of Physical Sciences

Evaluating lung cancer control through a time-delay mathematical model with detailed sensitivity analysis

Shah Zeb[a], Awais Ahmad[b], Rizwana Kausar[c], Siti Ainor Mohd Yatim[a,*], Nurulhuda Ramli[a,*], Muhammad Rafiq[d]

[a]School of Distance Education, Universiti Sains Malaysia, USM, 11800 Penang, Malaysia
[b]Department of Mathematics, Government College University Faisalabad, Faisalabad 38000, Pakistan
[c]School of Biological Sciences, Universiti Sains Malaysia, Minden, USM, 11800 Penang, Malaysia
[d]Department of Mathematics, Namal University, 30 km Talagang Road, Mianwali 42250, Pakistan

Abstract

Lung cancer (LC) is a leading cause of cancer-related deaths worldwide, posing a significant threat to public health due to its complex development, late diagnosis, and poor response to treatment. Rising rates, particularly among those exposed to tobacco consumption and environmental pollution, highlight the need for a realistic interpretation of disease dynamics through mathematical modeling. In this study, a nonlinear dynamical model of LC with time delay is formulated to represent the lag associated with smoking exposure and the evolution of smoking-related effects. The delay acts specifically through the delayed smoking-exposure interaction terms and does not represent treatment or immune response. The model is analyzed to confirm that solutions remain positive and bounded, ensuring biological feasibility. The basic reproduction number is calculated to describe threshold dynamics, and local stability of both the disease-free and endemic equilibrium is examined. Sensitivity analysis identifies the parameters influencing the model threshold quantity. The displayed analysis shows positive effects of θ, a, b, and e on $\Re_0$ and negative effects of d, g, m, and τ. These signs describe the mathematical sensitivity of the threshold quantity and do not establish treatment or recovery effects. Numerical simulations using nonstandard finite difference (NSFD), Euler, and fourth-order Runge–Kutta (RK4) methods validate the analytical results, with NSFD proving to be more stable and dynamically consistent. Findings suggest that government interventions, including tobacco control, education, and early screening awareness, can reduce the disease burden. These results offer insights for policymakers to develop cost-effective strategies.

DOI: 10.46481/jnsps.2026.3539

Keywords: Lung cancer, Basic reproduction number, Sensitivity analysis, Existence and uniqueness, Nonstandard finite difference

Article History:
Received: 21 May 2026
Received in revised form: 10 July 2026
Accepted for publication: 24 July 2026
Available online: 10 August 2026

Communicated by: B. J. Falaye

1. Introduction

Lung cancer (LC) accounts for over 2.1 million new cases and 1.8 million fatalities every year, making it one of the main causes of cancer-related deaths globally. About 80–90% of LC fatalities are caused by tobacco use, which is the main risk factor for the disease [1]. The incidence and prevalence of LC are significantly influenced by smoking recruitment rates, which are the rates at which new people start smoking. Time-delayed differential equations have been used to study smoking dynamics [28]. Experts in bio-mathematics, chronic-disease epidemiology, mathematical modeling, and simulation have conducted

*Corresponding authors Siti Ainor Mohd Yatim, Tel. No.: +60174484399. Nurulhuda Ramli, Tel. No.: +60193342425.

Email addresses: ainor@usm.my (Siti Ainor Mohd Yatim), rnurulhuda@usm.my (Nurulhuda Ramli)

numerous studies on progression dynamics [3]. Researchers can understand disease dynamics by mathematical modelling [4].

According to estimates, LC ranked first in terms of deaths and second in terms of new cases worldwide in 2018. With 13 to 15 lakh cancer patients and roughly 2 lakh new cases each year, Bangladesh, one of the most populous nations in the world, is at risk from the disease. Any aspect of the respiratory system may be affected by LC, which can originate anywhere in the lungs. Cancer cells, in contrast to normal cells, proliferate uncontrollably and devastate the surrounding healthy lung tissue. Through the process of metastasis into adjacent tissue or other body parts, this tumor may spread, or metastasize, from the lung to the lymph nodes [5].

Smoking tobacco is the primary cause of LC, accounting for approximately 80% of LC-related fatalities. Heart disease, chronic obstructive pulmonary disease (COPD), respiratory issues, cancer, premature birth, gum disease, tooth loss, eye problems, weakened bones, memory loss, and cognitive decline are among the other illnesses brought on by smoking. 28% of cancer-related deaths in the US are caused by LC, commonly known as bronchogenic carcinomas. The tracheobronchial system, which is made up of damaged cells found in our lungs and bronchial airways, is where LC develops [6]. This component of the human body is significant because inhaled air can pollute this system, which is a major contributing factor to the development of LC.

Asbestos and radon are examples of carcinogens, which scientists believe are the main cause of LC. However, studies and data indicate that tobacco smoke, which includes more than 60 carcinogens, is the primary cause of LC. Nowadays, a significant percentage of tobacco smoke-related deaths are caused by cigarette smoke. Approximately 400,000 Americans lose their lives to cigarette smoke each year, making up one in five deaths in the country [7]. Numerous factors, including the age at which smoking started, the duration of smoking, the quantity of cigarettes smoked daily, and the depth of inhalation, affect a smoker's risk of developing LC from cigarette smoke [8].

By emphasizing that nicotine and other ingredients in cigarettes were just as addictive as cocaine, the Surgeon General demonstrated the addictive potential of cigarette smoking in 1988. A smoker's addiction to nicotine makes it extremely difficult for them to stop. Actually, 90% of smokers want to stop but are unable to do so [9]. Only 34% of current smokers make an attempt to stop, and only 2.5% of them are successful each year, according to research. The single most avoidable cause of premature death in the US has been identified as cigarette usage and the harmful air it produces.

85–90% of all instances of LC (146,000 cases annually) have been linked to cigarette smoke. Additionally, an estimated 3,000 nonsmokers pass away from LC each year as a result of secondhand smoking, sometimes referred to as environmental tobacco smoke, or ETS. The U.S. Environmental Protection Agency claims that although the number of deaths among nonsmokers may be fewer than that of active smokers, it is still very high when compared to those linked to other indoor and outdoor environmental contaminants. Public measures that shield people from secondhand smoke have been greatly impacted by this evidence [10].

Because smoking spreads across the population, it is comparable to contagious diseases. Because of its conduct, the ratio of smoking-related diseases is rising every day. Johnston *et al.* [11] documented smoking behavior among secondary-school students, college students, and young adults. By including an additional class of mild smoking, Zaman, G. expanded and altered the work in Ref. [12]. The author of Ref. [13] concentrated on smoking control strategies by selecting the best control factors. Additionally, some smokers may continue to smoke while others may relapse as a result of frequent interaction with other smokers.

It is crucial to keep in mind that giving up smoking can significantly lower the chance of getting certain health issues and enhance general health and wellbeing. There are lots of tools available to assist you or someone you know stop smoking. You can begin by consulting a physician, contacting a support group, or using prescription drugs or nicotine replacement therapy to help you stop.

In this study, the dynamics of smoking were described by a linear ordinary differential equation of the SEIR model, which lacks a closed form solution. The majority of researchers used analytical solutions without an approximate outcome. Therefore, numerical simulation was used to examine how the factors and variables affect smoking-related LC dynamics [1]. A mathematical modeling strategy was employed in studying the dynamic and progression of smoking-related LC without taking a clinical approach into account. Several mathematical and computational techniques can be used to model the dynamics of smoking's effects on the lungs, such as Ordinary Differential Equations (ODEs), which describe the rates at which lung function and damage change over time. The spatial and temporal dynamics of lung injury and inflammation are modeled using partial differential equations (PDEs). Agent-Based Models (ABMs) are used to simulate how smoke particles, inflammatory chemicals, and lung cells interact. A network model that illustrates how various lung sections communicate and how damage spreads. Additionally, artificial intelligence (AI) and machine learning (ML) are utilized to analyze medical pictures and forecast declines in lung function.

Many mathematicians explored model-based research on LC in light of all the deaths caused by the disease. Numerous mathematical models of smoking behavior and LC have been put forth. Different researchers developed models to explain the population-level dynamics of LC brought on by smoking and secondhand smoke. According to these models, raising the number of people who are knowledgeable about the effects of smoking is the greatest method to reduce the number of smokers and people who develop LC. Current research includes work on liquid biopsy for LC and its implications for screening [14]. The creation of a blood test using multiplexed tumor-associated autoantibodies to identify non-small cell LC has also been investigated [15]. Trisilowati (2019) examines the stability and applies the optimal control method demonstrating that the optimal control is successful in limiting the growth of LC patients and passive and active smokers [16].

Research has also developed highly sensitive liquid-biopsy platforms for detecting clinically relevant cancer mutations at low allele fractions in cell-free DNA [17]. According to Beljanski *et al.* (2012), the main reason for clinical therapeutic treatment failure is multi-drug resistance. Compared to previous therapeutic treatments, genetically modified oncolytic viruses (OVs) attack tumor cells through entirely different methods. According to researchers' idea discussed in Ref. [18], treatments including OVs, which are currently being developed, may make it possible to overcome drug resistance and modify the immune response in order to combat cancer.

The SIRS Susceptible (S), Infected (I), Recovery (R), and Susceptible (S) model is an extension of the SIR (susceptible, Infected, Recovered) model, in which it is thought that people can contract coronavirus infections. Numerous researchers and epidemiologists have studied this model in an effort to prevent the disease from spreading further throughout the community. In an effort to better lower the number of sick persons and their potential to spread, the researchers developed a vaccine and immunized the majority of people. However, the globe is still dealing with infections in many nations due to the passage of time. Ref. [19] reports treatment strategies and outcomes in patients with synchronous multiple primary malignancies involving LC. Atangana examined the best control analysis for the eradication or management of COVID-19. Since the virus spreads quickly to other healthy people, isolation and quarantine are the best and most efficient ways to lessen the infection [20].

The primary cause of LC patients' high death rate is delayed detection, which results in inadequate curative therapy. Screening programs have been put in place all around the world to reduce the death rate from LC [21]. Early detection of LC improves the prognosis following surgery, however further research is required to fully comprehend metastatic LC [22], epidemiology, wave dynamics equations, etc. Using electronic cigarettes after quitting smoking increases the risk of LC [23]. The incidence rate is an important component of smoking models [13]. Thus, many smoking models with linear incidence rates [25], saturated incidence rates [26], square root type incidence rates [27], and harmonic mean type incidence rates [28] have been developed recently by researchers both domestically and internationally. Some others introduced age-structured smoking models [29] and fractional smoking models [30]. It is important to note that all of the aforementioned smoking models ignore the fact that snuffing is another way that tobacco is used [31]. Because of this, Alzahrani and Zeb developed the tobacco smoking model that includes the snuffing class [32].

Mathematical modeling-based studies on cancer progression are well documented but there is limited published work that addresses time-delay effects in LC dynamics and their influence on stability and control strategies. Many currently used models are based on classical ordinary differential equations, which usually ignore lags associated with smoking exposure and the evolution of smoking-related effects. Moreover, most studies have mainly qualitative analysis and do not consider delay-induced dynamics brought into the system evolution under physiological conditions. This limitation underscores the need for more comprehensive modeling frameworks that include time-delay effects to improve understanding of LC progression and control.

The current work extends previous deterministic cancer models by adding a biologically valid single time delay to the model system. Although the earlier models were able to establish critical properties like positivity/boundedness, equilibrium analysis and stability of both disease and endemic states, they did not consider a delay in the smoking-exposure interaction. LC is a non-communicable disease and is not contagious. The proposed model is based on the compartmental structure used as a mathematical model for describing the flow of individuals between smoking-related and disease-related compartments. Transitions between compartments do not, therefore, indicate infectious transmission, but rather transitions in disease development and the effects of smoking exposure. Our work, on the other hand, incorporates a delay term corresponding to the lag in smoking exposure and the evolution of smoking-related effects into the classical system, leading to a delay differential model. This extension also provides an opportunity for more thorough investigation of the effects delay can have on threshold dynamics, stability behavior, and long-term evolution of the system-phenomena that non-delayed models cannot adequately capture.

The mathematical soundness of the proposed delayed system is verified, through deriving core properties such as positivity, boundedness and an invariant region. We calculate the basic reproduction number as a measure of the threshold dynamics of the system, and to see if LC can continue or diminish in the population that we describe, and perform local as well as global stability analyses of the steady states using suitable analytical techniques. A forward sensitivity analysis is also undertaken to identify which parameters most strongly affect disease evolution, summarizing the relative influence of the model parameters on disease-progression dynamics. The sensitivity analysis can give valuable qualitative information about factors related to the progression of LC. In the present model, however, the variable of intervention, screening, treatment or policy-control is not explicitly incorporated. So any suggestions on prevention or disease management should be taken with a pinch of salt, and considered as possibilities for future research.

In the case of numerical simulations we use the NSFD method that is famous to maintain the qualitative properties of the dynamical systems including positivity and stability even when the step sizes are larger. The NSFD method maintained key qualitative characteristics of the underlying dynamical system and, in the numerical experiments analysed in this paper, showed to be more stable as the step size was increased than the corresponding Euler and RK4 schemes. All of the aforementioned items together, the time delay integration, the strict mathematical treatment, sensitivity exploration, and the application of the NSFD-based simulations are the key contributions of the study. These features can be more realistic and helpful with the description of the dynamics of LC and can give useful information in terms of developing effective, affordable, and sustainable intervention strategies.

The structure of this article is in the following way: Section 1 provides a general introduction to LC, its role in the world, and the latest advances of mathematical models and especially models with time-delays. Section 2 presents the proposed model, including the biological assumptions, descriptions of the model variables and parameters, and one time delay associated with smoking exposure and the evolution of smoking-related effects. Qualitative properties of the system are also determined in this section including the existence and uniqueness of solutions, positivity, boundedness, and the determination of equilibrium points. Moreover, the basic reproduction threshold is obtained, and local and global stability of the disease-free and endemic equilibria are studied with the help of proper mathematical methods.

Section 3 focuses on numerical simulations, with the dynamical behavior of the model being demonstrated with the help of suitable initial conditions and parameters. The effect of time delay on the stability of the system and the course of the disease is brought to the fore with the help of graphical data. In this part, the nonstandard finite difference (NSFD) method will be used because it can maintain the main qualitative characteristics of the system, giving biologically significant and stable solutions. The obtained results are also compared to the standard numerical methods to prove the effectiveness and reliability of the NSFD scheme. In Section 4, sensitivity analysis is performed in detail to understand how key parameters, particularly the delay term, affect the course of the disease. Last but not least, Section 5 sums up the study by creating a summary of key findings as well as highlighting how time delay can create an insight into the dynamics of LC. It also talks about practical implications of the findings especially on low resource settings and also gives recommendations on where future research can be directed to enhance modeling techniques and control measures.

2. Materials and methods

2.1. Delay mathematical model

LC is among the severe and life-threatening illnesses in the whole world and it kills a large number of individuals annually and specifically in the developed and developing nations. Contrary to infectious diseases, LC emerges over a long period as a result of the prolonged exposure of an individual to the risk factors of smoking, air pollution, and work hazards. Thus, delay modeling is relevant to the course of the modeled process because smoking-related effects may emerge after a lag following exposure. Whereas LC cannot be fully prevented, its risk can be minimized through preventive measures, early diagnosis and medical treatments. A delay factor can be used to represent the lag between smoking exposure and the evolution of smoking-related effects represented by the delayed interaction terms. The work in the present study is based on a mathematical framework, which already exists and appropriate control measures to study the interaction between susceptible persons and individuals at various LC stages.

- S(t) describes the susceptible class.
- M(t) describes the active-smoker class.
- V(t) describes the smoking-victim class.
- C(t) describes the LC class.
- R(t) describes the recovered class.

Considering a total population N(t) at any time t which is subdivided into five compartments such as, The compartment (S) refers to those people who could be exposed to smoking-related health risks, but who have not yet experienced complications from smoking. The compartment (M) represents the group of active smokers, the ones who are directly exposed to tobacco. The compartment (V) is for passive smokers or those who are strongly exposed to the carcinogenic factors in cigarette smoke. The compartment (C) is for those with a diagnosis of LC and (R) is for those who have been treated and cured or achieved remission. The transitions between compartments are smoking behaviors, effects of exposure to smoking, progression of diseases, and recovery processes, but not person-to-person disease transmission. The delay parameter τ corresponds to the time lag that is seen in smoking exposure and the evolution of smoking related effects which may play a part in the progression of LC. The interaction terms $S(t-\tau)M(t-\tau)$ are particularly interesting because the bad effects of smoking do not appear immediately but after some time of exposure. Thus, the delay is not actually the time required to become infected with the disease but rather represents processes related to behavior and exposure.

$$N(t) = S(t) + M(t) + V(t) + C(t) + R(t). \tag{1}$$

In the model above, a and b represent the rates at which vulnerable populations become active and passive smokers, respectively, and θ and m represent the population's natural growth and mortality rates.

$$\frac{dS}{dt} = \theta - aM(t-\tau)S(t-\tau)e^{-m\tau} - bM(t-\tau)S(t-\tau)e^{-m\tau} - mS(t) + hR(t).$$

The delayed direct transition in the susceptible compartment is represented by $e^{-m\tau}$. The interaction between passive and active smokers is not considered, and e represents the rate at which passive smokers become active smokers.

$$\frac{dM}{dt} = aM(t-\tau)S(t-\tau)e^{-m\tau} + eV(t) - gM(t) - mM(t).$$

The constants g and d denote the rates at which active and passive smokers contract LC.

$$\frac{dV}{dt} = bM(t-\tau)S(t-\tau)e^{-m\tau} - eV(t) - dV(t) - mV(t).$$

The variable ϕ denotes the recovery rate from LC with appropriate treatment, while f signifies the mortality rate generated by the disease.

$$\frac{dC}{dt} = gM(t) + dV(t) - \phi C(t) - (m+f)C(t).$$

Table 1: Parameter and variable values used in the SMVCR lung cancer model.

Parameter	Description	Value	Reference
θ	Growth rate of the population	0.05 d^{-1}	[33]
m	Natural mortality rate	0.01 d^{-1}	[33]
a	Active-smoker recruitment rate from the susceptible population	0.25 d^{-1}	[33]
b	Rate at which the population becomes a victim of smoking	0.75 d^{-1}	[33]
e	Rate at which the population migrates from the victim group to smokers	0.35 d^{-1}	[33]
g	Smoker's LC incidence rate	0.2 d^{-1}	[33]
d	LC incidence rate from the victim group	0.05 d^{-1}	[33]
ϕ	LC recovery rate	0.2 d^{-1}	[33]
f	Cancer incidence mortality rate	0.6 d^{-1}	[33]
h	Migration rate from the recovered to susceptible compartments	0.5 d^{-1}	[33]
τ	Time delay	≥ 0	Assumed

In reality, individuals who have received therapy and recovered from LC may remain vulnerable to a recurrence, with the incidence rate represented by h.

$$\frac{dR}{dt} = \phi C(t) - (m + h)R(t).$$

The parameters utilized in the numerical and graphical analysis of the model are presented in Table 1.

A set of delay differential equations for the following mathematical model.

$$\begin{aligned}
\frac{dS}{dt} &= \theta - aM(t-\tau)S(t-\tau)e^{-m\tau} \\
&\quad - bM(t-\tau)S(t-\tau)e^{-m\tau} - mS(t) + hR(t), \qquad (2)\\
\frac{dM}{dt} &= aM(t-\tau)S(t-\tau)e^{-m\tau} + eV(t) - gM(t) - mM(t), \qquad (3)\\
\frac{dV}{dt} &= bM(t-\tau)S(t-\tau)e^{-m\tau} - eV(t) - dV(t) - mV(t), \qquad (4)\\
\frac{dC}{dt} &= gM(t) + dV(t) - \phi C(t) - (m + f)C(t), \qquad (5)\\
\frac{dR}{dt} &= \phi C(t) - (m + h)R(t), \qquad (6)
\end{aligned}$$

given initial conditions

$$S > 0, \quad M \geq 0, \quad V \geq 0, \quad C \geq 0, \quad R \geq 0. \qquad (7)$$

Here, t ≥ 0. $\quad \tau \leq t$.

2.2. Model analysis

The proposed mathematical framework analyzes the qualitative aspects of the process of LC progression. The basic properties of the system like existence, boundedness, and stability of the equilibrium points are rigorously studied to get an insight into the long-term behavior of the system. Such analyses play a crucial role in the development of the disease and whether effective control measures can be implemented or not. In addition, an appropriate threshold parameter, analogous to a basic reproduction number in an epidemiological model, is calculated to characterize persistence or decline of the smoking-related and LC compartments. The time-delay factor represents the lag in smoking exposure and the evolution of smoking-related effects through the delayed interaction terms. Therefore, the model provides a framework for analyzing relationships among the population compartments defined above.

Theorem 2.1. The proposed delayed model has nonnegative solution for all $t \geq 0$ if the initial history functions are nonnegative on $[-\tau, 0]$.

Proof. Suppose that the history functions of the delayed system are nonnegative and continuous.

$$\begin{aligned}
S(\xi) &= \psi_1(\xi), & M(\xi) &= \psi_2(\xi),\\
V(\xi) &= \psi_3(\xi), & C(\xi) &= \psi_4(\xi),\\
R(\xi) &= \psi_5(\xi).
\end{aligned}$$

for

$$\xi \in [-\tau, 0],$$

where

$$\psi_i(\xi) \geq 0, \qquad i = 1, 2, 3, 4, 5.$$

$$\frac{dS}{dt} = \theta - aMSe^{-m\tau} - bMSe^{-m\tau} - mS + hR.$$

As all state variables are non-negative we have $R(t) \geq 0$, and therefore.

$$\frac{dS}{dt} \geq \theta - (aM(t)e^{-m\tau} + bM(t)e^{-m\tau} + m)S(t).$$

Let

$$B(t) = aM(t)e^{-m\tau} + bM(t)e^{-m\tau} + m.$$

Then the inequality above is reduced to

$$\frac{dS}{dt} \geq \theta - B(t)S(t).$$

Multiplying both sides by the integrating factor

$$\exp\left(\int_0^t B(s)\,ds\right),$$

we obtain

$$\frac{d}{dt}\left[S(t)\exp\left(\int_0^t B(s)\,ds\right)\right] \geq \theta\exp\left(\int_0^t B(s)\,ds\right).$$

Integrating from 0 to t,

$$S(t)\exp\left(\int_0^t B(s)\,ds\right) - S(0) \geq \theta\int_0^t \exp\left(\int_0^w B(s)\,ds\right)dw.$$

Hence,

$$S(t) \geq S(0)\exp\left(-\int_0^t B(s)\,ds\right) + \theta\exp\left(-\int_0^t B(s)\,ds\right)\int_0^t \exp\left(\int_0^w B(s)\,ds\right)dw.$$

As the exponential is strictly positive and $\theta > 0$, then it follows that

$$S(t) > 0 \quad \text{for all } t > 0.$$

The other state variables M(t), V(t), C(t), and R(t) can be handled equally: they all obey a linear equations with non-negative inflow due to a compartment that has already been found to be positive or due to a positive source term. So, assuming that they are non-negative, they are strictly positive at any $t > 0$. □

Theorem 2.2. The solutions of the equations are all confined within a feasible region.

Proof. The total population is indicated by the combination of all differential equations $N(t)$.

$$\frac{dN}{dt} = \frac{dS}{dt} + \frac{dM}{dt} + \frac{dV}{dt} + \frac{dC}{dt} + \frac{dR}{dt}.$$

When the equations' right-hand sides are substituted, we obtain

$$\frac{dN}{dt} = \theta - mN(t) - fC,$$

since $C(t) \geq 0$, it follows that

$$\frac{dN}{dt} \leq \theta - mN(t).$$

The above is a linear differential inequality. The corresponding linear differential equation

$$\frac{dN}{dt} = \theta - mN(t)$$

has the solution

$$N(t) \leq \frac{\theta}{m} + \left(N(0) - \frac{\theta}{m}\right)e^{-mt}, \qquad t \geq 0.$$

Hence, we obtain

$$0 \leq N(t) \leq \max\left\{N(0), \frac{\theta}{m}\right\}, \qquad \text{for all } t \geq 0.$$

Therefore, the feasible region is given by

$$\Omega = \left\{(S, M, V, C, R) \in \mathbb{R}_+^5 : S + M + V + C + R \leq \max\left\{N(0), \frac{\theta}{m}\right\}\right\}.$$

Thus, all solutions of the model are bounded in Ω. □

2.3. Model equilibrium point

The model's admission of a disease-free equilibrium and an endemic equilibrium, respectively, characterize the absence and persistence of LC. The feasible region contains the disease-free equilibrium, which represents a population free of cancer. An endemic equilibrium is reached when the fundamental reproduction number is greater than unity and denotes persistence of LC-related compartments in the modeled population. These equilibrium points serve as the foundation for both the model's stability and long-term dynamical study.

2.3.1. DFE point

The DFE points are:

$$\varepsilon_0 = (S_0, M_0, V_0, C_0, R_0) = \left(\frac{\theta}{m}, 0, 0, 0, 0\right).$$

2.3.2. Reproduction number

The dynamics of the proposed LC model are evaluated using a threshold parameter analogous to the basic reproduction number in epidemiological systems. In this population-compartment model, M, V, and C denote active smokers, victims of smoking, and individuals with LC, respectively, while S and R denote susceptible and recovered individuals. The threshold quantity characterizes persistence of the smoking-related and LC compartments under the modeled transitions; it does not represent infectious transmission or the creation of malignant cells. The next-generation matrix methodology is used here as a mathematical device for the defined compartmental transition structure.

For this construction, $x = (M, V, C)$ collects the smoking-related and LC compartments used in the next-generation calculation, whereas $y = (S, R)$ collects the remaining compartments. The vector $F(x, y)$ represents new entries into the selected compartments generated by the delayed smoking-exposure interaction terms, and $V(x, y)$ represents transfers among and out of those compartments. Consequently, the system can be stated as

$$\frac{dx}{dt} = F(x, y) - V(x, y),$$

From the linearization of the system at the disease-free equilibrium (DFE), the matrices F and V are obtained.

The threshold parameter, denoted by $\mathfrak{R}_0$, is obtained as the spectral radius of the next-generation matrix FV^{-1}. This value defines a threshold for the modeled population compartments:

when $\mathfrak{R}_0 < 1$, the smoking-related and LC compartments decline near the DFE, whereas $\mathfrak{R}_0 > 1$ indicates persistence near the threshold. Stability of the equilibrium points is highly related to the value of $\mathfrak{R}_0$. In particular, the DFE is locally asymptotic in case of $\mathfrak{R}_0 < 1$ and is unstable in case of $\mathfrak{R}_0 > 1$. To verify these conditions of stability the Jacobian matrix of the system evaluated at the DFE is used too. At the DFE, the matrices are

$$F = \begin{bmatrix} \frac{a\theta e^{-m\tau}}{m} & 0 & 0 \\ \frac{b\theta e^{-m\tau}}{m} & 0 & 0 \\ 0 & 0 & 0 \end{bmatrix},$$

and

$$V = \begin{bmatrix} g+m & -e & 0 \\ 0 & m+e+d & 0 \\ -g & -d & m+f+\phi \end{bmatrix}.$$

Hence, the next-generation matrix is

$$FV^{-1} = \begin{bmatrix} \frac{a\theta e^{-m\tau}}{m(g+m)} & \frac{a\theta e\, e^{-m\tau}}{m(g+m)(m+e+d)} & 0 \\ \frac{b\theta e^{-m\tau}}{m(g+m)} & \frac{b\theta e\, e^{-m\tau}}{m(g+m)(m+e+d)} & 0 \\ 0 & 0 & 0 \end{bmatrix}.$$

The characteristic equation of FV^{-1} is

$$\det(FV^{-1} - \lambda I) = 0,$$

which gives, the $\mathfrak{R}_0$ is the spectral radius of FV^{-1}, therefore

$$\mathfrak{R}_0 = \rho(FV^{-1}) = \frac{\theta e^{-m\tau}}{m(g+m)}\left(a + \frac{be}{m+e+d}\right). \tag{8}$$

2.3.3. EE point

The EE points are:

$$\varepsilon_1 = (S_1, M_1, V_1, C_1, R_1) = (S^*, M^*, V^*, C^*, R^*).$$

This implies that,

$$\begin{aligned} S^* &= \frac{\theta + hR^*}{aM^*e^{-m\tau} + bM^*e^{-m\tau} + m}, \\ M^* &= \frac{eV^*}{g+m-aS^*e^{-m\tau}}, \\ V^* &= \frac{bM^*S^*e^{-m\tau}}{e+d+m}, \\ C^* &= \frac{gM^* + dV^*}{\phi+m+f}, \\ R^* &= \frac{\phi C^*}{m+h}. \end{aligned}$$

Biology requires all the components of the equilibrium to be positive. In particular, given the expression M^* of the condition

$$g + m - aS^*e^{-m\tau} > 0$$

must hold. With this restriction and positivity of all the parameters in the model, the endemic equilibrium is positive and biologically relevant.

2.4. Stability analysis

This section examines local asymptotic stability (LAS) and global asymptotic stability (GAS) at the DFE and EE.

Theorem 2.3. The system at $\varepsilon_0 = (S_0, M_0, V_0, C_0, R_0) = \left(\frac{\theta}{m}, 0, 0, 0, 0\right)$ is LAS if $\mathfrak{R}_0 < 1$.

Proof. The Jacobian matrix of the system is

$$J = \begin{bmatrix} -(a+b)Me^{-m\tau} - m & -(a+b)Se^{-m\tau} & 0 & 0 & h \\ aMe^{-m\tau} & aSe^{-m\tau} - g - m & e & 0 & 0 \\ bMe^{-m\tau} & bSe^{-m\tau} & -e-d-m & 0 & 0 \\ 0 & g & d & -(\phi+m+f) & 0 \\ 0 & 0 & 0 & \phi & -(m+h) \end{bmatrix}.$$

Evaluating the Jacobian at the disease-free equilibrium

$$\varepsilon_0 = \left(\frac{\theta}{m}, 0, 0, 0, 0\right),$$

gives

$$J(\varepsilon_0) = \begin{bmatrix} -m & -(a+b)\frac{\theta}{m}e^{-m\tau} & 0 & 0 & h \\ 0 & a\frac{\theta}{m}e^{-m\tau} - g - m & e & 0 & 0 \\ 0 & b\frac{\theta}{m}e^{-m\tau} & -e-d-m & 0 & 0 \\ 0 & g & d & -(\phi+m+f) & 0 \\ 0 & 0 & 0 & \phi & -(m+h) \end{bmatrix}.$$

The characteristic equation is obtained from

$$\det(\lambda I - J(\varepsilon_0)) = 0.$$

Since the first column contains only one nonzero entry, the determinant can be written as

$$\det(\lambda I - J(\varepsilon_0)) = (\lambda + m)\det(A),$$

where

$$A = \begin{bmatrix} \lambda - \left(a\frac{\theta}{m}e^{-m\tau} - g - m\right) & -e & 0 & 0 \\ -b\frac{\theta}{m}e^{-m\tau} & \lambda+e+d+m & 0 & 0 \\ -g & -d & \lambda+\phi+m+f & 0 \\ 0 & 0 & -\phi & \lambda+m+h \end{bmatrix}.$$

Expanding along the last column yields

$$\det(A) = (\lambda + m + h)\det(B),$$

where

$$B = \begin{bmatrix} \lambda - \left(a\frac{\theta}{m}e^{-m\tau} - g - m\right) & -e & 0 \\ -b\frac{\theta}{m}e^{-m\tau} & \lambda+e+d+m & 0 \\ -g & -d & \lambda+\phi+m+f \end{bmatrix}.$$

Again expanding along the third column, we obtain

$$\det(B) = (\lambda+\phi+m+f)\left[(\lambda-\alpha)(\lambda+\beta) - be\frac{\theta}{m}e^{-m\tau}\right],$$

where

$$\alpha = a\frac{\theta}{m}e^{-m\tau} - g - m, \qquad \beta = e + d + m.$$

Hence, the characteristic polynomial becomes

$$(\lambda+m)(\lambda+m+h)(\lambda+\phi+m+f)\left[(\lambda-\alpha)(\lambda+\beta) - be\frac{\theta}{m}e^{-m\tau}\right] = 0.$$

Therefore, three eigenvalues are immediately obtained as

$$\lambda_1 = -m, \qquad \lambda_2 = -(m+h), \qquad \lambda_3 = -(\phi+m+f),$$

which are all negative since every model parameter is positive. The remaining two eigenvalues satisfy

$$\lambda^2 + (\beta-\alpha)\lambda - \alpha\beta - be\frac{\theta}{m}e^{-m\tau} = 0.$$

By the Routh–Hurwitz criterion for a quadratic polynomial, both roots have negative real parts if

$$\beta - \alpha > 0,$$

and

$$-\alpha\beta - be\frac{\theta}{m}e^{-m\tau} > 0.$$

These inequalities are equivalent to the threshold condition

$$\mathfrak{R}_0 < 1.$$

Hence, all eigenvalues of the Jacobian matrix have negative real parts whenever $\mathfrak{R}_0 < 1$. By the Linearization (Hartman-Grobman) Theorem, the DFE ε_0 is LAS. Therefore, the DFE is LAS whenever $\mathfrak{R}_0 < 1$. □

Theorem 2.4. The system at $\varepsilon_1 = (S_1, M_1, V_1, C_1, R_1) = (S^*, M^*, V^*, C^*, R^*)$ is LAS if $\mathfrak{R}_0 > 1$.

Proof. The Jacobian matrix evaluated at the endemic equilibrium ε_1 is

$$J(\varepsilon_1) = \begin{bmatrix} -(a+b)M^*e^{-m\tau} - m & -(a+b)S^*e^{-m\tau} & 0 & 0 & h \\ aM^*e^{-m\tau} & aS^*e^{-m\tau} - g - m & e & 0 & 0 \\ bM^*e^{-m\tau} & bS^*e^{-m\tau} & -e-d-m & 0 & 0 \\ 0 & g & d & -(\phi+m+f) & 0 \\ 0 & 0 & 0 & \phi & -(m+h) \end{bmatrix}.$$

The characteristic equation is obtained from

$$\det(\lambda I - J(\varepsilon_1)) = 0,$$

which can be written as

$$\lambda^5 + a_1\lambda^4 + a_2\lambda^3 + a_3\lambda^2 + a_4\lambda + a_5 = 0,$$

where the coefficients a_1, a_2, a_3, a_4 and a_5 depend on the model parameters and the endemic equilibrium values S^*, M^*, V^*, C^* and R^*. Since all model parameters are positive and the endemic equilibrium exists only when $\mathfrak{R}_0 > 1$, it follows that

$$a_i > 0, \qquad i = 1, 2, \ldots, 5.$$

By the Routh–Hurwitz criterion, all roots of the characteristic polynomial have negative real parts provided that

$$a_1 > 0, \qquad a_2 > 0, \qquad a_3 > 0, \qquad a_4 > 0, \qquad a_5 > 0,$$

together with

$$a_1a_2 > a_3,$$
$$a_1a_2a_3 > a_1^2a_4 + a_3^2,$$

and

$$(a_1a_2 - a_3)(a_3a_4 - a_2a_5) > (a_1a_4 - a_5)^2.$$

These inequalities are satisfied whenever $\mathfrak{R}_0 > 1$, since the endemic equilibrium is biologically feasible and all coefficients of the characteristic polynomial remain positive. Hence, all eigenvalues of the Jacobian matrix have negative real parts. Therefore, by the Hartman-Grobman (Linearization) Theorem, the endemic equilibrium ε_1 is LAS. Thus, The endemic equilibrium ε_1 is LAS $\mathfrak{R}_0 > 1$. □

Theorem 2.5. The system at $\varepsilon_0 = (S_0, M_0, V_0, C_0, R_0) = \left(\frac{\theta}{m}, 0, 0, 0, 0\right)$ is GAS if $\mathfrak{R}_0 < 1$.

Proof. Consider the Lyapunov function

$$L = M + \frac{e}{m+e+d}V + C + R.$$

Differentiating along solutions gives

$$\dot{L} = \dot{M} + \frac{e}{m+e+d}\dot{V} + \dot{C} + \dot{R}.$$

Substituting the system equations yields

$$\begin{aligned}\dot{L} = {} & aMSe^{-m\tau} - (g+m)M \\ & + \frac{e}{m+e+d}\left(bMSe^{-m\tau} - (m+e+d)V\right) \\ & + gM + dV - (\phi+m+f)C + \phi C - (m+h)R.\end{aligned}$$

Simplifying,

$$\begin{aligned}\dot{L} = {} & \left[\left(a + \frac{be}{m+e+d}\right)Se^{-m\tau} - (g+m)\right]M \\ & - mV - (m+f)C - (m+h)R.\end{aligned}$$

Using the invariant bound $S(t) \le \frac{\theta}{m}$, we obtain

$$\begin{aligned}\dot{L} \le {} & \left[\frac{\theta e^{-m\tau}}{m}\left(a + \frac{be}{m+e+d}\right) - (g+m)\right]M \\ & - mV - (m+f)C - (m+h)R.\end{aligned}$$

Rewriting in terms of $\mathfrak{R}_0$,

$$\dot{L} \le (g+m)(\mathfrak{R}_0 - 1)M - mV - (m+f)C - (m+h)R.$$

Hence, if $\mathfrak{R}_0 < 1$, then

$$\dot{L} \le 0.$$

Moreover, $\dot{L} = 0$ implies

$$M = V = C = R = 0.$$

On this invariant set, the system reduces to

$$\frac{dS}{dt} = \theta - mS,$$

which has a unique equilibrium $S = \frac{\theta}{m}$. Thus, the largest invariant set in $\{\dot{L} = 0\}$ is

$$\left\{\left(\frac{\theta}{m}, 0, 0, 0, 0\right)\right\}.$$

By LaSalle's Invariance Principle, every solution in Ω converges to ε_0. Therefore, the DFE is GAS whenever $\mathfrak{R}_0 < 1$. □

Theorem 2.6. The system at $\varepsilon_1 = (S_1, M_1, V_1, C_1, R_1) = (S^*, M^*, V^*, C^*, R^*)$ is GAS if $\mathfrak{R}_0 > 1$.

Proof. To prove this theorem, we consider the previously constructed Lyapunov function at ε_1 as follows:

$$\begin{aligned} V = {} & W_1\left(S - S^* - S^* \ln \frac{S}{S^*}\right) + W_2\left(M - M^* - M^* \ln \frac{M}{M^*}\right) \\ & + W_3\left(V - V^* - V^* \ln \frac{V}{V^*}\right) + W_4\left(C - C^* - C^* \ln \frac{C}{C^*}\right) \\ & + W_5\left(R - R^* - R^* \ln \frac{R}{R^*}\right). \end{aligned}$$

where $W_1, \ldots, W_5$ are positive constants to be determined.

$$\begin{aligned} \frac{dV}{dt} = {} & W_1\left(1 - \frac{S^*}{S}\right)\frac{dS}{dt} + W_2\left(1 - \frac{M^*}{M}\right)\frac{dM}{dt} \\ & + W_3\left(1 - \frac{V^*}{V}\right)\frac{dV}{dt} + W_4\left(1 - \frac{C^*}{C}\right)\frac{dC}{dt} \\ & + W_5\left(1 - \frac{R^*}{R}\right)\frac{dR}{dt}. \end{aligned}$$

By substituting the derivative value

$$\begin{aligned} \frac{dV}{dt} = {} & W_1\left(1 - \frac{S^*}{S}\right)(\theta - aMS e^{-m\tau} - bMS e^{-m\tau} - mS + hR) \\ & + W_2\left(1 - \frac{M^*}{M}\right)(aMS e^{-m\tau} + eV - gM - mM) \\ & + W_3\left(1 - \frac{V^*}{V}\right)(bMS e^{-m\tau} - eV - dV - mV) \\ & + W_4\left(1 - \frac{C^*}{C}\right)(gM + dV - \phi C - (m + f)C) \\ & + W_5\left(1 - \frac{R^*}{R}\right)(\phi C - (m + h)R). \end{aligned}$$

After simplification,

$$\begin{aligned} \frac{dV}{dt} = {} & W_1(S - S^*)\left(\frac{\theta}{S} - aMe^{-m\tau} - bMe^{-m\tau} - m + \frac{hR}{S}\right) \\ & + W_2(M - M^*)\left(aS e^{-m\tau} + \frac{eV}{M} - g - m\right) \\ & + W_3(V - V^*)\left(\frac{bMS e^{-m\tau}}{V} - e - d - m\right) \\ & + W_4(C - C^*)\left(\frac{gM}{C} + \frac{dV}{C} - \phi - (m + f)\right) \\ & + W_5(R - R^*)\left(\frac{\phi C}{R} - (m + h)\right). \end{aligned}$$

Since, $\varepsilon_1 = (S^*, M^*, V^*, C^*, R^*)$

$$\frac{dS^*}{dt} = \frac{dM^*}{dt} = \frac{dV^*}{dt} = \frac{dC^*}{dt} = \frac{dR^*}{dt} = 0.$$

Hence,

$$\begin{aligned} m &= \frac{\theta}{S} - aMe^{-m\tau} - bMe^{-m\tau} + \frac{hR}{S}, \\ g + m &= aS e^{-m\tau} + \frac{eV}{M}, \\ e + d + m &= \frac{bMS e^{-m\tau}}{V}, \\ m + f &= \frac{gM}{C} + \frac{dV}{C} - \phi, \\ m + h &= \frac{\phi C}{R}. \end{aligned}$$

So,

$$\begin{aligned} \frac{dV}{dt} = {} & W_1(S - S^*)\left[\frac{\theta}{S} - aMe^{-m\tau} - bMe^{-m\tau}\right. \\ & \left. - \left(\frac{\theta}{S} - aMe^{-m\tau} - bMe^{-m\tau} + \frac{hR}{S}\right) + \frac{hR}{S}\right] \\ & + W_2(M - M^*)\left[aS e^{-m\tau} + \frac{eV}{M} - \left(aS e^{-m\tau} + \frac{eV}{M}\right)\right] \\ & + W_3(V - V^*)\left[\frac{bMS e^{-m\tau}}{V} - \frac{bMS e^{-m\tau}}{V}\right] \\ & + W_4(C - C^*)\left[\frac{gM}{C} + \frac{dV}{C} - \phi - \left(\frac{gM}{C} + \frac{dV}{C} - \phi\right)\right] \\ & + W_5(R - R^*)\left[\frac{\phi C}{R} - \frac{\phi C}{R}\right]. \end{aligned}$$

For simplicity, we take

$$W_1 = W_2 = W_3 = W_4 = W_5 = 1.$$

We get,

$\frac{dV}{dt} \leq 0$, *where*, $\mathfrak{R}_0 > 1$.

The feasible set is positively bounded and invariant. Consequently, the system is GAS at EE point ε_1. □

3. Numerical simulations

The present paper addresses the dynamical nature of the suggested system through the use of various numerical schemes. Specifically, Euler and fourth-order Runge–Kutta (RK4) methods are utilized in numerically studying the system. Moreover, the non-standard finite difference (NSFD) scheme is used to guarantee a higher degree of stability and dynamical consistency of the model. Such a comparison of these numerical methods is useful in analyzing qualitative behavior and accuracy of the solutions of the system.

3.1. Forward Euler scheme

$$S^{n+1} = S^n + h\left(\theta - aM^nS^ne^{-m\tau} - bM^nS^ne^{-m\tau} - mS^n + hR^n\right), \tag{9}$$

$$M^{n+1} = M^n + h\left(aM^nS^ne^{-m\tau} + eV^n - gM^n - mM^n\right), \tag{10}$$

$$V^{n+1} = V^n + h\left(bM^nS^ne^{-m\tau} - eV^n - dV^n - mV^n\right), \tag{11}$$

$$C^{n+1} = C^n + h\left(gM^n + dV^n - \phi C^n - (m+f)C^n\right), \tag{12}$$

$$R^{n+1} = R^n + h\left(\phi C^n - (m+h)R^n\right). \tag{13}$$

3.2. Fourth-order Runge–Kutta (RK4) method

$$\begin{aligned}
k_1 &= h\left(\theta - aM^nS^ne^{-m\tau} - bM^nS^ne^{-m\tau} - mS^n + hR^n\right),\\
l_1 &= h\left(aM^nS^ne^{-m\tau} + eV^n - gM^n - mM^n\right),\\
n_1 &= h\left(bM^nS^ne^{-m\tau} - eV^n - dV^n - mV^n\right),\\
o_1 &= h\left(gM^n + dV^n - \phi C^n - (m+f)C^n\right),\\
p_1 &= h\left(\phi C^n - (m+h)R^n\right),
\end{aligned}$$

$$\begin{aligned}
k_2 &= h\Big[\theta - a\left(M^n + \frac{l_1}{2}\right)\left(S^n + \frac{k_1}{2}\right)e^{-m\tau}\\
&\quad - b\left(M^n + \frac{l_1}{2}\right)\left(S^n + \frac{k_1}{2}\right)e^{-m\tau}\\
&\quad - m\left(S^n + \frac{k_1}{2}\right) + h\left(R^n + \frac{p_1}{2}\right)\Big],\\
l_2 &= h\Big[a\left(M^n + \frac{l_1}{2}\right)\left(S^n + \frac{k_1}{2}\right)e^{-m\tau}\\
&\quad + e\left(V^n + \frac{n_1}{2}\right) - g\left(M^n + \frac{l_1}{2}\right) - m\left(M^n + \frac{l_1}{2}\right)\Big],\\
n_2 &= h\Big[b\left(M^n + \frac{l_1}{2}\right)\left(S^n + \frac{k_1}{2}\right)e^{-m\tau}\\
&\quad - e\left(V^n + \frac{n_1}{2}\right) - d\left(V^n + \frac{n_1}{2}\right) - m\left(V^n + \frac{n_1}{2}\right)\Big],\\
o_2 &= h\Big[g\left(M^n + \frac{l_1}{2}\right) + d\left(V^n + \frac{n_1}{2}\right)\\
&\quad - \phi\left(C^n + \frac{o_1}{2}\right) - (m+f)\left(C^n + \frac{o_1}{2}\right)\Big],\\
p_2 &= h\Big[\phi\left(C^n + \frac{o_1}{2}\right) - (m+h)\left(R^n + \frac{p_1}{2}\right)\Big].
\end{aligned}$$

$$\begin{aligned}
k_3 &= h\Big[\theta - a\left(M^n + \frac{l_2}{2}\right)\left(S^n + \frac{k_2}{2}\right)e^{-m\tau}\\
&\quad - b\left(M^n + \frac{l_2}{2}\right)\left(S^n + \frac{k_2}{2}\right)e^{-m\tau}\\
&\quad - m\left(S^n + \frac{k_2}{2}\right) + h\left(R^n + \frac{p_2}{2}\right)\Big],\\
l_3 &= h\Big[a\left(M^n + \frac{l_2}{2}\right)\left(S^n + \frac{k_2}{2}\right)e^{-m\tau}\\
&\quad + e\left(V^n + \frac{n_2}{2}\right) - g\left(M^n + \frac{l_2}{2}\right) - m\left(M^n + \frac{l_2}{2}\right)\Big],\\
n_3 &= h\Big[b\left(M^n + \frac{l_2}{2}\right)\left(S^n + \frac{k_2}{2}\right)e^{-m\tau}\\
&\quad - e\left(V^n + \frac{n_2}{2}\right) - d\left(V^n + \frac{n_2}{2}\right) - m\left(V^n + \frac{n_2}{2}\right)\Big],\\
o_3 &= h\Big[g\left(M^n + \frac{l_2}{2}\right) + d\left(V^n + \frac{n_2}{2}\right)\\
&\quad - \phi\left(C^n + \frac{o_2}{2}\right) - (m+f)\left(C^n + \frac{o_2}{2}\right)\Big],\\
p_3 &= h\Big[\phi\left(C^n + \frac{o_2}{2}\right) - (m+h)\left(R^n + \frac{p_2}{2}\right)\Big].
\end{aligned}$$

$$\begin{aligned}
k_4 &= h\Big[\theta - a(M^n + l_3)(S^n + k_3)e^{-m\tau}\\
&\quad - b(M^n + l_3)(S^n + k_3)e^{-m\tau} - m(S^n + k_3) + h(R^n + p_3)\Big],\\
l_4 &= h\Big[a(M^n + l_3)(S^n + k_3)e^{-m\tau} + e(V^n + n_3)\\
&\quad - g(M^n + l_3) - m(M^n + l_3)\Big],\\
n_4 &= h\Big[b(M^n + l_3)(S^n + k_3)e^{-m\tau} - e(V^n + n_3)\\
&\quad - d(V^n + n_3) - m(V^n + n_3)\Big],\\
o_4 &= h\Big[g(M^n + l_3) + d(V^n + n_3) - \phi(C^n + o_3)\\
&\quad - (m+f)(C^n + o_3)\Big],\\
p_4 &= h\left[\phi(C^n + o_3) - (m+h)(R^n + p_3)\right].
\end{aligned}$$

thus, the ultimate results are,

$$S^{n+1} = S^n + \frac{1}{6}(k_1 + 2k_2 + 2k_3 + k_4). \tag{14}$$

$$M^{n+1} = M^n + \frac{1}{6}(l_1 + 2l_2 + 2l_3 + l_4). \tag{15}$$

$$V^{n+1} = V^n + \frac{1}{6}(n_1 + 2n_2 + 2n_3 + n_4). \quad (16)$$

$$C^{n+1} = C^n + \frac{1}{6}(o_1 + 2o_2 + 2o_3 + o_4). \quad (17)$$

$$R^{n+1} = R^n + \frac{1}{6}(p_1 + 2p_2 + 2p_3 + p_4). \quad (18)$$

3.3. Nonstandard finite difference method

This section will discuss how NSFD approach of model is stable at the DFE point.

$$S^{n+1} = \frac{S^n + h_1\theta + h_1 h R^n}{1 + h_1 a M^n e^{-m\tau} + h_1 b M^n e^{-m\tau} + h_1 m}. \quad (19)$$

$$M^{n+1} = \frac{M^n + h_1 e V^n}{1 + h_1 g + h_1 m - h_1 a S^n e^{-m\tau}}. \quad (20)$$

$$V^{n+1} = \frac{V^n + h_1 b M^n S^n e^{-m\tau}}{1 + h_1 e + h_1 d + h_1 m}. \quad (21)$$

$$C^{n+1} = \frac{C^n + h_1 g M^n + h_1 d V^n}{1 + h_1\phi + h_1(m + f)}. \quad (22)$$

$$R^{n+1} = \frac{R^n + h_1\phi C^n}{1 + h_1(m + h)}. \quad (23)$$

In order for NSFD scheme to preserve nonnegative numerical solution, the denominators in the update equations are required to be positive. In particular, from equation (20),

$$1 + h_1 g + h_1 m - h_1 a S^n e^{-m\tau} > 0.$$

Thus the step size and model parameters are selected to satisfy the above throughout the simulations. With this constraint the NSFD scheme maintains the positive nature of state variables.

3.4. Convergence analysis of the NSFD scheme

With an emphasis on the DFE point, the convergence of the NSFD technique used on the model will be examined in this section. This is the NSFD scheme's Jacobian.

$$J(\varepsilon_0) = \begin{bmatrix} \frac{1}{1+h_1 m} & -\frac{(\frac{\theta}{m}+h_1\theta)h_1(a+b)e^{-m\tau}}{(1+h_1 m)^2} & 0 & 0 & \frac{h_1 h}{1+h_1 m} \\ 0 & \frac{1}{1+h_1 g+h_1 m-\frac{h_1 a\theta}{m}e^{-m\tau}} & \frac{h_1 e}{1+h_1 g+h_1 m-\frac{h_1 a\theta}{m}e^{-m\tau}} & 0 & 0 \\ 0 & \frac{h_1 b\frac{\theta}{m}e^{-m\tau}}{1+h_1 e+h_1 d+h_1 m} & \frac{1}{1+h_1 e+h_1 d+h_1 m} & 0 & 0 \\ 0 & \frac{h_1 g}{1+h_1\phi+h_1(m+f)} & \frac{h_1 d}{1+h_1\phi+h_1(m+f)} & \frac{1}{1+h_1\phi+h_1(m+f)} & 0 \\ 0 & 0 & 0 & \frac{h_1\phi}{1+h_1(m+h)} & \frac{1}{1+h_1(m+h)} \end{bmatrix}.$$

The eigenvalues may be determined through the diagonal and sub-block matrices of the Jacobian matrix because of the block triangular structure. Therefore, the eigenvalues of $(J(\varepsilon_0))$ are found to be

$\lambda_1 = \frac{1}{1+h_1 m}$, $\lambda_4 = \frac{1}{1+h_1\phi+h_1(m+f)}$, $\lambda_5 = \frac{1}{1+h_1(m+h)}$, and $\lambda_{2,3} = \frac{(J_{22}+J_{33}) \pm \sqrt{(J_{22}+J_{33})^2 - 4(J_{22}J_{33} - J_{23}J_{32})}}{2}$,

$$J_{22} = \frac{1}{1 + h_1 g + h_1 m - \frac{h_1 a\theta}{m}e^{-m\tau}},$$

$$J_{23} = \frac{h_1 e}{1 + h_1 g + h_1 m - \frac{h_1 a\theta}{m}e^{-m\tau}},$$

$$J_{32} = \frac{h_1 b\frac{\theta}{m}e^{-m\tau}}{1 + h_1 e + h_1 d + h_1 m},$$

$$J_{33} = \frac{1}{1 + h_1 e + h_1 d + h_1 m}.$$

Having all the model parameters positive, $(h_1 > 0)$ follows that $\lambda_1 < 1$, $\lambda_4 < 1$ and $\lambda_5 < 1$. The DFE is thus stable based on the roots $\lambda_{2,3}$. In the event that all the eigenvalues meet conditions of $|\lambda_i| < 1$, (i=1,2,3,4,5), then the DFE (ε_0) is LAS.

3.5. Positivity analysis

Theorem 3.1. Suppose that at $t = 0$, S, M, V, C, and R, the variables of the NSFD scheme, are positive; moreover, if all the variables are positive, then $S^{n+1} \geq 0$, $M^{n+1} \geq 0$, $V^{n+1} \geq 0$, $C^{n+1} \geq 0$, and $R^{n+1} \geq 0$.

Proof. Taking into account the NSFD schemes of the variables S,M,V,C, and R (19)–(23) as:

$$S^{n+1} = \frac{S^n + h_1\theta + h_1 h R^n}{1 + h_1 a M^n e^{-m\tau} + h_1 b M^n e^{-m\tau} + h_1 m}.$$

$$M^{n+1} = \frac{M^n + h_1 e V^n}{1 + h_1 g + h_1 m - h_1 a S^n e^{-m\tau}}.$$

$$V^{n+1} = \frac{V^n + h_1 b M^n S^n e^{-m\tau}}{1 + h_1 e + h_1 d + h_1 m}.$$

$$C^{n+1} = \frac{C^n + h_1 g M^n + h_1 d V^n}{1 + h_1\phi + h_1(m + f)}.$$

$$R^{n+1} = \frac{R^n + h_1\phi C^n}{1 + h_1(m + h)}.$$

By combining all of the equations in the system that was previously examined with n=0, we arrive at the following expression.

$$S^1 = \frac{S^0 + h_1\theta + h_1 h R^0}{1 + h_1 a M^0 e^{-m\tau} + h_1 b M^0 e^{-m\tau} + h_1 m} \geq 0,$$

$$M^1 = \frac{M^0 + h_1 e V^0}{1 + h_1 g + h_1 m - h_1 a S^0 e^{-m\tau}} \geq 0,$$

$$V^1 = \frac{V^0 + h_1 b M^0 S^0 e^{-m\tau}}{1 + h_1 e + h_1 d + h_1 m} \geq 0,$$

$$C^1 = \frac{C^0 + h_1 g M^0 + h_1 d V^0}{1 + h_1\phi + h_1(m + f)} \geq 0,$$

$$R^1 = \frac{R^0 + h_1\phi C^0}{1 + h_1(m + h)} \geq 0.$$

Now that n=1 has been entered, we can proceed to the following stage.

$$S^2 = \frac{S^1 + h_1\theta + h_1 h R^1}{1 + h_1 a M^1 e^{-m\tau} + h_1 b M^1 e^{-m\tau} + h_1 m} \geq 0,$$

$$M^2 = \frac{M^1 + h_1 e V^1}{1 + h_1 g + h_1 m - h_1 a S^1 e^{-m\tau}} \geq 0,$$

$$V^2 = \frac{V^1 + h_1 b M^1 S^1 e^{-m\tau}}{1 + h_1 e + h_1 d + h_1 m} \geq 0,$$

$$C^2 = \frac{C^1 + h_1 g M^1 + h_1 d V^1}{1 + h_1\phi + h_1(m + f)} \geq 0,$$

$$R^2 = \frac{R^1 + h_1\phi C^1}{1 + h_1(m+h)} \geq 0.$$

For n=2,3,4,...,n-1, let the phrase $S^{n+1} \geq 0, M^{n+1} \geq 0, V^{n+1} \geq 0, C^{n+1} \geq 0, R^{n+1} \geq 0$; stay positive. We will determine whether a random positive integer n in Z is positive. We discover that

$$S^{n+1} = \frac{S^n + h_1\theta + h_1hR^n}{1 + h_1aM^ne^{-m\tau} + h_1bM^ne^{-m\tau} + h_1m} \geq 0,$$
$$M^{n+1} = \frac{M^n + h_1eV^n}{1 + h_1g + h_1m - h_1aS^ne^{-m\tau}} \geq 0,$$
$$V^{n+1} = \frac{V^n + h_1bM^nS^ne^{-m\tau}}{1 + h_1e + h_1d + h_1m} \geq 0,$$
$$C^{n+1} = \frac{C^n + h_1gM^n + h_1dV^n}{1 + h_1\phi + h_1(m+f)} \geq 0,$$
$$R^{n+1} = \frac{R^n + h_1\phi C^n}{1 + h_1(m+h)} \geq 0.$$

Consequently, the suggested methodology guarantees the positivity of the state variables S, M, V, C, and R for any positive integer values of n. □

3.6. Boundedness of the NSFD scheme

Theorem 3.2. Let S^0, M^0, V^0, C^0 and R^0 be finite, so that $S^0 + M^0 + V^0 + C^0 + R^0 \leq 1$. Furthermore, under the model θ, b, g, d, h, ϕ are all positive. Then, $S^{n+1}, M^{n+1}, V^{n+1}, C^{n+1}$ and R^{n+1} are bounded by the specified real fixed value c_{n+1} such that $S^{n+1}, M^{n+1}, V^{n+1}, C^{n+1}$ and $R^{n+1} < c_{n+1}\ \forall\ n \in Z^+$ where $c_{n+1} = c_n + h_1\theta + h_1bc_n^2 + h_1(g + d + h + \phi + e)c_n$. and $c_1 = 1 + h_1\theta + h_1(bS^0M^0 + gM^0 + dV^0 + hR^0)$.

Proof. The state variables of the NSFD scheme are S, M, V, C, and R (19)–(23),

$$S^{n+1}(1 + h_1aM^ne^{-m\tau} + h_1bM^ne^{-m\tau} + h_1m) = S^n + h_1\theta + h_1hR^n,$$
$$M^{n+1}(1 + h_1g + h_1m - h_1aS^ne^{-m\tau}) = M^n + h_1eV^n,$$
$$V^{n+1}(1 + h_1e + h_1d + h_1m) = V^n + h_1bM^nS^ne^{-m\tau},$$
$$C^{n+1}(1 + h_1\phi + h_1(m+f)) = C^n + h_1gM^n + h_1dV^n,$$
$$R^{n+1}(1 + h_1(m+h)) = R^n + h_1\phi C^n.$$

Adding all the above equations then

$S^{n+1} + M^{n+1} + V^{n+1} + C^{n+1} + R^{n+1} + S^{n+1}(h_1aM^ne^{-m\tau} + h_1bM^ne^{-m\tau} + h_1m) + M^{n+1}(h_1g + h_1m - h_1aS^ne^{-m\tau}) + V^{n+1}(h_1e + h_1d + h_1m) + C^{n+1}(h_1\phi + h_1(m + f)) + R^{n+1}h_1(m+h) = S^n + h_1\theta + h_1hR^n + M^n + h_1eV^n + V^n + h_1bM^nS^ne^{-m\tau} + C^n + h_1gM^n + h_1dV^n + R^n + h_1\phi C^n,$

$S^{n+1} + M^{n+1} + V^{n+1} + C^{n+1} + R^{n+1} + S^{n+1}(h_1aM^ne^{-m\tau} + h_1bM^ne^{-m\tau} + h_1m) + M^{n+1}(h_1g + h_1m - h_1aS^ne^{-m\tau}) + V^{n+1}(h_1e + h_1d + h_1m) + C^{n+1}(h_1\phi + h_1(m+f)) + R^{n+1}h_1(m+h) = S^n + M^n + V^n + C^n + R^n + h_1\theta + h_1hR^n + h_1eV^n + h_1bM^nS^ne^{-m\tau} + h_1gM^n + h_1dV^n + h_1\phi C^n.$ (24)

Substituting n=0 into equation (24), we obtain

$S^1 + M^1 + V^1 + C^1 + R^1 + S^1\left(h_1aM^0e^{-m\tau} + h_1bM^0e^{-m\tau} + h_1m\right) + M^1(h_1g + h_1m - h_1aS^0e^{-m\tau}) + V^1(h_1e + h_1d + h_1m) + C^1(h_1\phi + h_1(m+f)) + R^1h_1(m+h) = S^0 + M^0 + V^0 + C^0 + R^0 + h_1\theta + h_1hR^0 + h_1eV^0 + h_1bM^0S^0e^{-m\tau} + h_1gM^0 + h_1dV^0 + h_1\phi C^0,$

$S^1 + M^1 + V^1 + C^1 + R^1 + S^1\left(h_1aM^0e^{-m\tau} + h_1bM^0e^{-m\tau} + h_1m\right) + M^1(h_1g + h_1m - h_1aS^0e^{-m\tau}) + V^1(h_1e + h_1d + h_1m) + C^1(h_1\phi + h_1(m+f)) + R^1h_1(m+h) < c_1$

$(S^1 + M^1 + V^1 + C^1 + R^1) + S^1\left(h_1aM^0e^{-m\tau} + h_1bM^0e^{-m\tau} + h_1m\right) + M^1(h_1g + h_1m - h_1aS^0e^{-m\tau}) + V^1(h_1e + h_1d + h_1m) + C^1(h_1\phi + h_1(m+f)) + R^1h_1(m+h) < 1 + h_1\theta + h_1(bS^0M^0 + gM^0 + dV^0 + hR^0)$

$$S^1 < c_1,$$
$$M^1 < c_1,$$
$$V^1 < c_1,$$
$$C^1 < c_1,$$
$$R^1 < c_1,$$

by substituting n=1 into equation (24), we obtain:

$(S^2 + M^2 + V^2 + C^2 + R^2) + S^2\left(h_1aM^1e^{-m\tau} + h_1bM^1e^{-m\tau} + h_1m\right) + M^2(h_1g + h_1m - h_1aS^1e^{-m\tau}) + V^2(h_1e + h_1d + h_1m) + C^2(h_1\phi + h_1(m+f)) + R^2h_1(m+h) < c_2,$

$$S^2 < c_2,$$
$$M^2 < c_2,$$
$$V^2 < c_2,$$
$$C^2 < c_2,$$
$$R^2 < c_2,$$

assume that for some $n \geq 1$,

$$S^n < c_n, \quad M^n < c_n, \quad V^n < c_n, \quad C^n < c_n, \quad R^n < c_n.$$
$$(S^{n+1} + M^{n+1} + V^{n+1} + C^{n+1} + R^{n+1}) + \cdots < c_{n+1},$$
$$S^{n+1} < c_{n+1},$$
$$M^{n+1} < c_{n+1},$$
$$V^{n+1} < c_{n+1},$$
$$C^{n+1} < c_{n+1},$$
$$R^{n+1} < c_{n+1}.$$

As a result, all positive values of $S^{n+1}, M^{n+1}, V^{n+1}, C^{n+1}$, and R^{n+1} are limited to a real number represented by c_{n+1}. □

3.7. Consistency analysis

The consistency of our numerical method is examined using Taylor's series expansion. Initially, we apply Taylor's series expansion on S^{n+1} and the Susceptible equation of the numerical integration model.

$$S^{n+1} = S^n + h_1\frac{dS}{dt} + \frac{h_1^2}{2!}\frac{d^2S}{dt^2} + \frac{h_1^3}{3!}\frac{d^3S}{dt^3} + \dots$$

From equation (3.11) we get,

$$\left(S^n + h_1\frac{dS}{dt} + \frac{h_1^2}{2!}\frac{d^2S}{dt^2} + \frac{h_1^3}{3!}\frac{d^3S}{dt^3} + \dots\right) \times (1 + h_1 aM^n e^{-m\tau} + h_1 bM^n e^{-m\tau} + h_1 m) = S^n + h_1\theta + h_1 hR^n.$$

$$\begin{aligned} &S^n + S^n h_1\left(aM^n e^{-m\tau} + bM^n e^{-m\tau} + m\right) \\ &+ h_1\frac{dS}{dt}\left(1 + h_1 aM^n e^{-m\tau} + h_1 bM^n e^{-m\tau} + h_1 m\right) \\ &+ \frac{h_1^2}{2!}\frac{d^2S}{dt^2}\left(1 + h_1 aM^n e^{-m\tau} + h_1 bM^n e^{-m\tau} + h_1 m\right) \\ &+ \frac{h_1^3}{3!}\frac{d^3S}{dt^3}\left(1 + h_1 aM^n e^{-m\tau} + h_1 bM^n e^{-m\tau} + h_1 m\right) + \dots \\ &= S^n + h_1\theta + h_1 hR^n. \end{aligned}$$

The result of applying $h_1 \to 0$ is as follows

$$S^n\left(aM^n e^{-m\tau} + bM^n e^{-m\tau} + m\right) + \frac{dS}{dt} = \theta + hR^n,$$

Rearrange the formula

$$\frac{dS}{dt} = \theta - aM^n S^n e^{-m\tau} - bM^n S^n e^{-m\tau} - mS^n + hR^n.$$

Our equation is congruent with the model equation (2), as demonstrated by the above equation. The final equation is then obtained by applying the same procedure to M^{n+1},

$$\frac{dM}{dt} = aMSe^{-m\tau} + eV - gM - mM.$$

Given that the same procedure applies to V^{n+1}, we obtain

$$\frac{dV}{dt} = bMSe^{-m\tau} - eV - dV - mV.$$

Given that the same procedure applies to C^{n+1}, we obtain

$$\frac{dC}{dt} = gM + dV - \phi C - (m + f)C.$$

Given that the same procedure applies to R^{n+1}, we obtain

$$\frac{dR}{dt} = \phi C - (m + h)R.$$

So the NSFD scheme is consistent with the underlying continuous model as $h_1 \to 0$. This analysis helps to establish the first-order consistency of the scheme but is not a rigorous proof of convergence.

3.8. Numerical analysis

The numerical simulations were performed with the parameter values given in Table 1 and initial conditions

$$(S(0), M(0), V(0), C(0), R(0)) = (0.3, 0.25, 0.1, 0.2, 0.15).$$

The value of the delay parameter was set to $\tau = 10$ while the computational step size was chosen as $h = 2.5$ and the simulations were performed for $0 \le t \le 500$ in Figure 1. With the parameter setting used in the baseline, the basic reproduction number is $\mathfrak{R}_0 > 1$ and the scenario of the endemic equilibrium is considered in the numerical experiment.

Numerical study of the dynamical behavior of the proposed system is performed based on three different discretization schemes which include the Euler, the classical fourth-order Runge–Kutta ($RK4$) method and the nonstandard finite difference (NSFD) scheme. Even though Euler and RK4 are popular because of their simplicity and accuracy, they do not usually maintain important qualitative characteristics of the continuous system, particularly when time step size is large as shown in Figure 2. Conversely, the NSFD approach is designed in a way that it preserves the key characteristics like positivity, boundedness and dynamical consistency. The numerical comparison shows that the NSFD scheme is better than the classical methods since it is not prone to spurious oscillations and instability, hence more accurate and biologically viable solutions. These findings substantiate the claim that NSFD is a sound and stable scheme in modeling nonlinear dynamical systems with time-delays.

The result indicates that the NSFD method is still convergent and dynamically consistent while the Euler and RK4 methods are unstable and divergent for $h = 3.8$. This illustrates a better numerical stability of the NSFD scheme for the delayed LC model proposed.

4. Discussion and analysis by parameters

In this section we carry out sensitivity analysis to find out how the model parameters influence the $\mathfrak{R}_0$. It aids in identifying the parameters that most strongly influence the model threshold quantity. Through the analysis of the sensitivity indices we get to know how a very slight change in a parameter affects the value of $\mathfrak{R}_0$. The forward sensitivity of the $\mathfrak{R}_0$ in a parameter P is normalized and is defined as.

$$Sensitivity\ Analysis = \frac{\partial \mathfrak{R}_0}{\partial P} \times \frac{P}{\mathfrak{R}_0}$$

Positive effect on $\mathfrak{R}_0$:

$$\frac{\partial \mathfrak{R}_0}{\partial \theta} = \frac{e^{-m\tau}}{m(g+m)}\left(a + \frac{be}{m+e+d}\right) > 0 \ \text{(positive effect)}$$

$$\frac{\partial \mathfrak{R}_0}{\partial a} = \frac{\theta e^{-m\tau}}{m(g+m)} > 0 \ \text{(positive effect)}$$

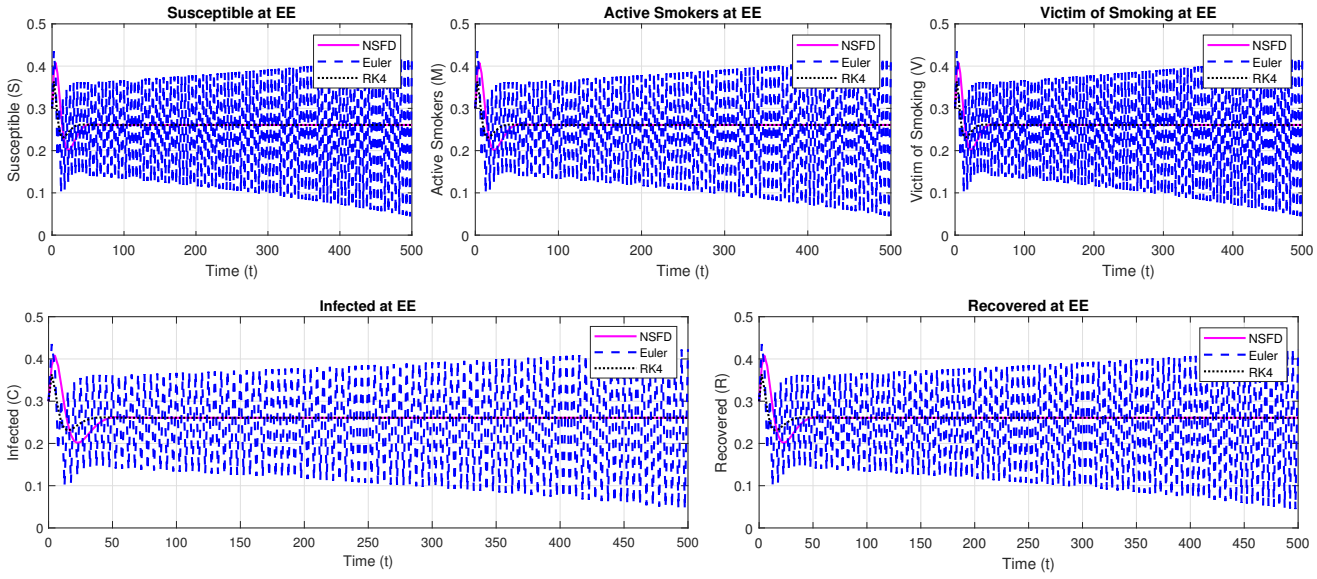

Figure 1: Comparison of the Euler, RK4, and NSFD methods.

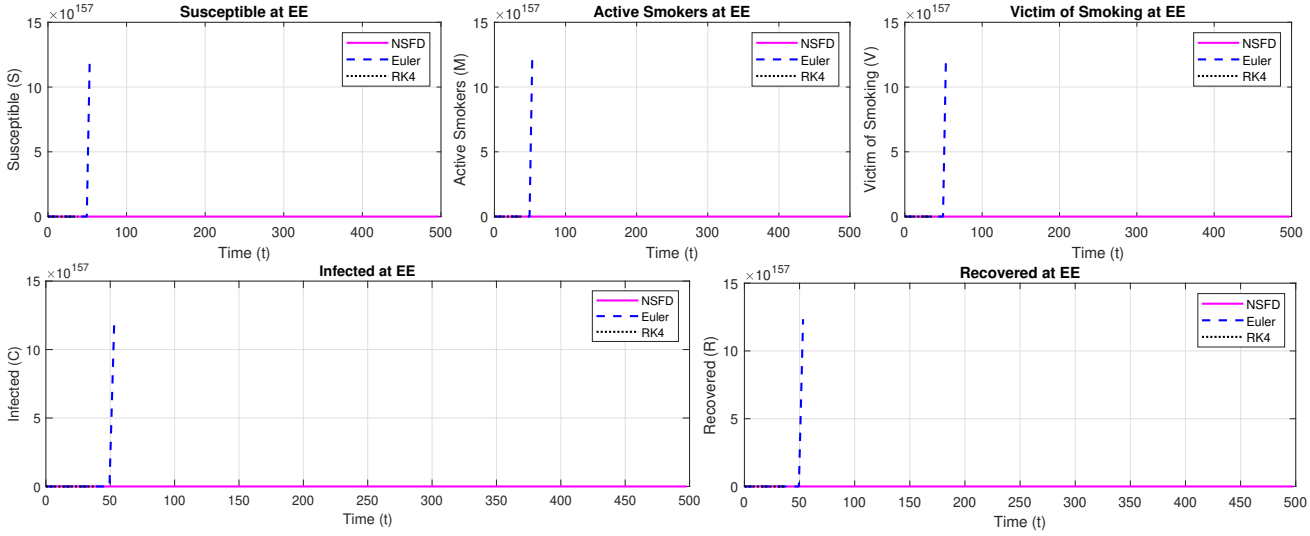

Figure 2: Comparison of the Euler, RK4, and NSFD methods.

$$\frac{\partial \mathfrak{R}_0}{\partial b} = \frac{\theta e^{-m\tau}}{m(g+m)}\left(\frac{e}{m+e+d}\right) > 0 \text{ (positive effect)}$$

$$\frac{\partial \mathfrak{R}_0}{\partial e} = \frac{\theta e^{-m\tau}}{m(g+m)}\left(\frac{b(m+d)}{(m+e+d)^2}\right) > 0 \text{ (positive effect)}$$

Negative effect on $\mathfrak{R}_0$:

$$\frac{\partial \mathfrak{R}_0}{\partial d} = -\frac{\theta e^{-m\tau}}{m(g+m)}\left(\frac{be}{(m+e+d)^2}\right) < 0 \text{ (negative effect)}$$

$$\frac{\partial \mathfrak{R}_0}{\partial g} = -\frac{\theta e^{-m\tau}}{m(g+m)^2}\left(a + \frac{be}{m+e+d}\right) < 0 \text{ (negative effect)}$$

$$\frac{\partial \mathfrak{R}_0}{\partial m} = -\frac{\theta e^{-m\tau}}{m^2(g+m)}\left(a + \frac{be}{m+e+d}\right) - \frac{\theta e^{-m\tau}}{m(g+m)^2}\left(a + \frac{be}{m+e+d}\right) - \frac{\theta\tau e^{-m\tau}}{m(g+m)}\left(a + \frac{be}{m+e+d}\right) - \frac{\theta e^{-m\tau}}{m(g+m)}\left(\frac{be}{(m+e+d)^2}\right) < 0$$

$$\frac{\partial \mathfrak{R}_0}{\partial \tau} = -m\mathfrak{R}_0 < 0$$

The normalized sensitivity indices shown in Figure 3 are consistent with the displayed analysis: θ, a, b, and e have positive effects on $\mathfrak{R}_0$, whereas d, g, m, and τ have negative effects.

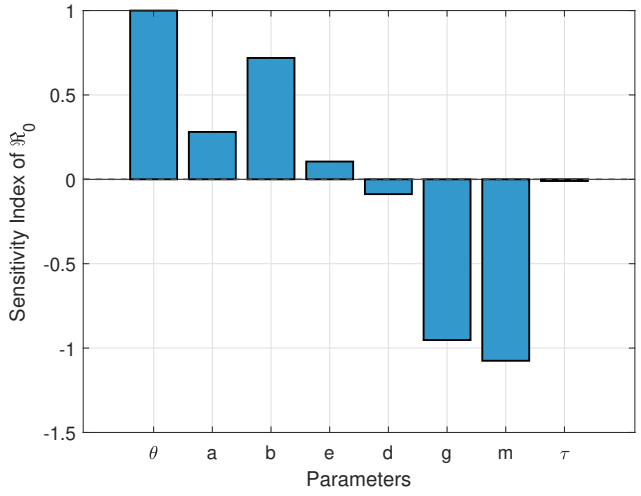

Figure 3: Sensitivity index values.

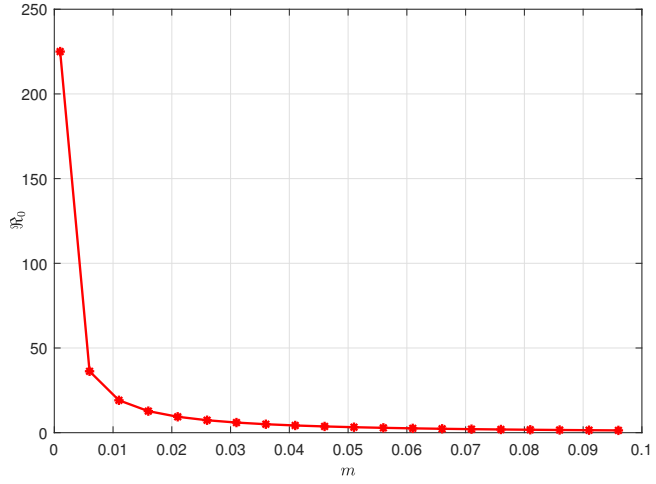

Figure 4: Relationship between $\mathfrak{R}_0$ and the natural mortality rate.

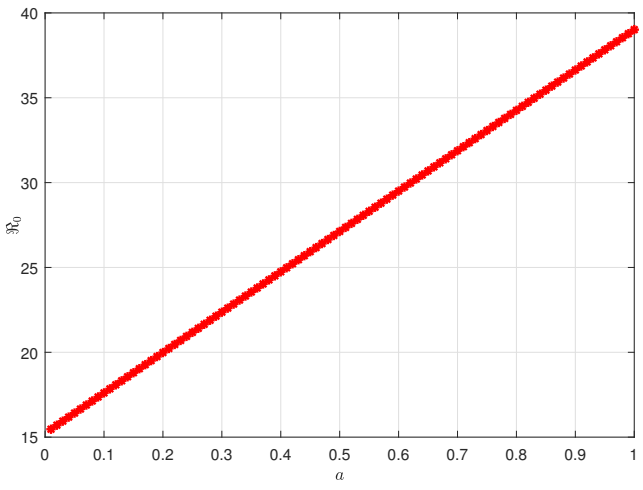

Figure 5: Relationship between $\mathfrak{R}_0$ and the active-smoker recruitment rate from the susceptible population.

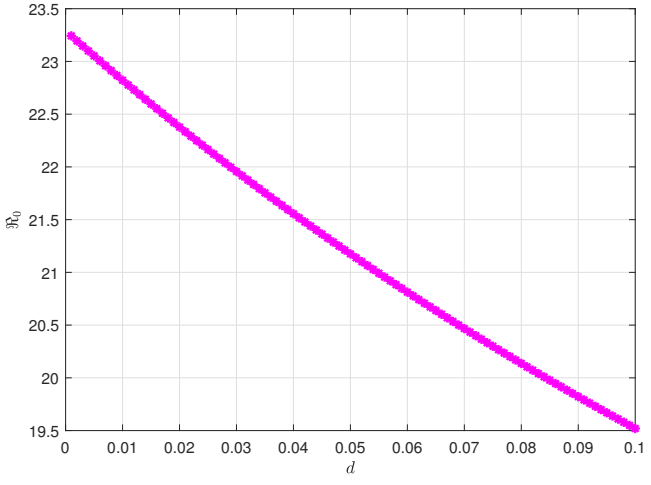

Figure 6: Relationship between $\mathfrak{R}_0$ and the LC incidence rate from the victim group.

These signs describe the mathematical response of the threshold quantity. In particular, the negative sensitivities of g and d arise from the structure of $\mathfrak{R}_0$ and should not be interpreted as reductions in the overall burden of LC.

In Figure 4, the higher the value of m, the larger the denominator of $\mathfrak{R}_0$ and the smaller the threshold quantity. This is a monotonic effect of natural mortality on the displayed threshold.

An increase in a increases $\mathfrak{R}_0$ because it adds to the population of active smokers. Figure 5 shows a monotonic increase in the model threshold with active-smoker recruitment.

An increase in d also leads to a slight reduction in $\mathfrak{R}_0$ because d appears in the denominator of the second term in $\mathfrak{R}_0$. Figure 6 therefore shows a mathematical decrease in the displayed threshold quantity; this should not be interpreted as a reduction in LC burden.

As indicated in the Figure 7, the increase in b will result in the increase in $\mathfrak{R}_0$ due to more people becoming victims and turning into smokers. This implies that forming of the victim has a direct positive impact on the $\mathfrak{R}_0$.

In Figure 8, an increase in g decreases $\mathfrak{R}_0$ because g appears in the denominator of $\mathfrak{R}_0$. This shows a decreasing trend in the model threshold quantity.

In Figure 9, an increment in e means an increment in $\mathfrak{R}_0$ as more victims move into the smoker compartment. The curve therefore illustrates a positive relationship between this migration parameter and the threshold quantity.

An increase in τ causes a decrease in $\mathfrak{R}_0$ through the factor $e^{-m\tau}$. Figure 10 indicates that increasing the exposure-related delay decreases the threshold quantity.

Figure 11 shows how $\mathfrak{R}_0$ and b relate to each other at varying values of the delay parameter τ. The value of $\mathfrak{R}_0$ increases with b, whereas increasing τ decreases $\mathfrak{R}_0$ through the exponential factor. This shows the dampening effect of the delay on the modeled threshold dynamics.

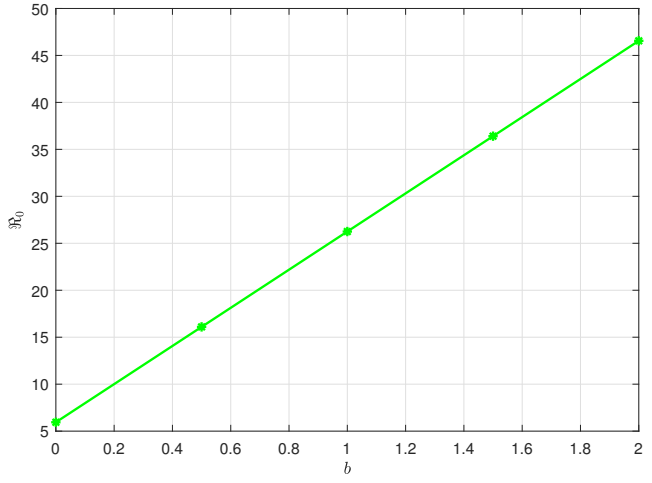

Figure 7: Relationship between $\mathfrak{R}_0$ and the rate at which the population becomes a victim of smoking.

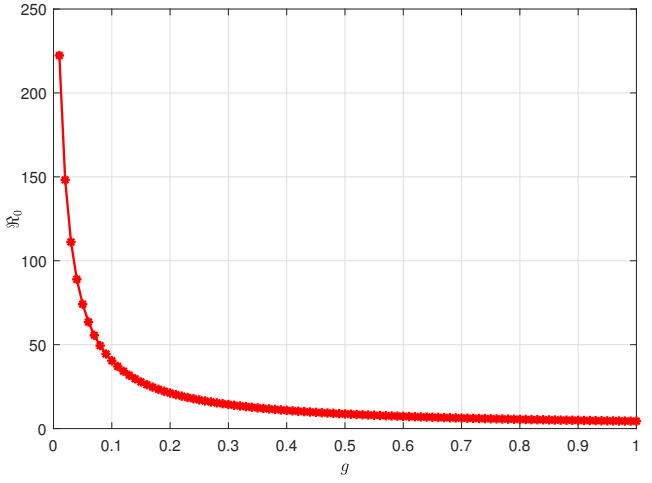

Figure 8: Relationship between $\mathfrak{R}_0$ and the smoker's LC incidence rate.

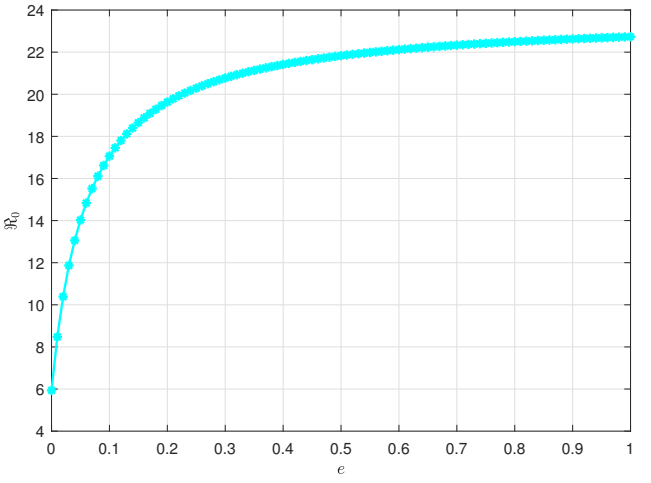

Figure 9: Relationship between $\mathfrak{R}_0$ and the rate at which the population migrates from the victim group to smokers.

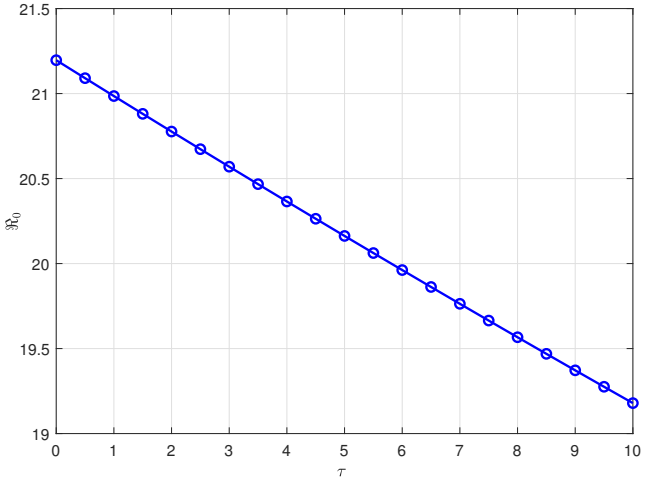

Figure 10: Relationship between $\mathfrak{R}_0$ and the time delay.

Figure 12 shows how $\mathfrak{R}_0$ varies with respect to parameter b assuming that the susceptible population S has different values. As shown, the greater the value of b, the greater the plotted value of $\mathfrak{R}_0$. Furthermore, the plotted value of $\mathfrak{R}_0$ increases with the assumed value of S. Under the varied-S interpretation used in this figure, increases in S and b therefore increase the plotted threshold quantity.

The surface in Figure 13 shows the parameters a and b against $\mathfrak{R}_0$ in three dimensions. The value of $\mathfrak{R}_0$ increases as either a or b increases, showing a positive relationship between active-smoker recruitment, smoking victimization, and the model threshold quantity.

The three-dimensional surface plot in Figure 14 shows how the parameter b and delay parameter τ jointly affect $\mathfrak{R}_0$. The value of $\mathfrak{R}_0$ increases with b and decreases as τ increases because of the exponential decay factor $e^{-m\tau}$. Thus, the delay decreases the displayed threshold quantity.

The sensitivity and numerical analyses show that the analyzed parameters can substantially affect the model threshold quantity and LC-related compartmental dynamics. Among the parameters included in the displayed sensitivity analysis, θ, a, b, and e have positive effects on $\mathfrak{R}_0$, whereas d, g, m, and τ have negative effects. These signs describe the mathematical response of $\mathfrak{R}_0$ and do not establish beneficial treatment or recovery effects. The delay parameter acts through the smoking-exposure interaction terms, and increasing τ decreases $\mathfrak{R}_0$ through the factor $e^{-m\tau}$. Thus, the results support interpreting the delay as an exposure-related lag rather than a treatment- or immune-response delay.

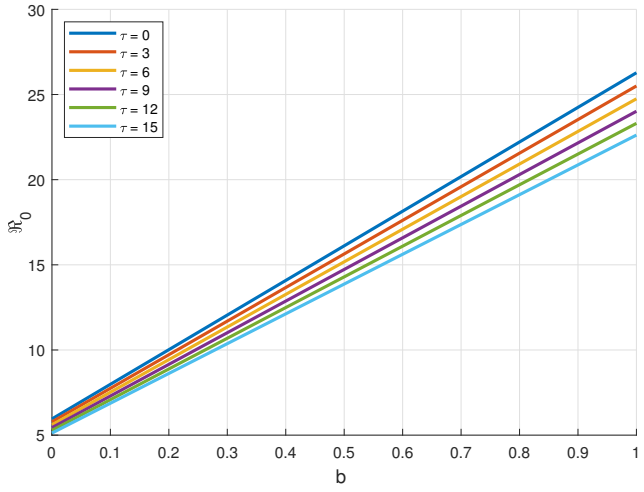

Figure 11: Combined effect of the rate at which the population becomes a victim of smoking and the delay on $\mathfrak{R}_0$.

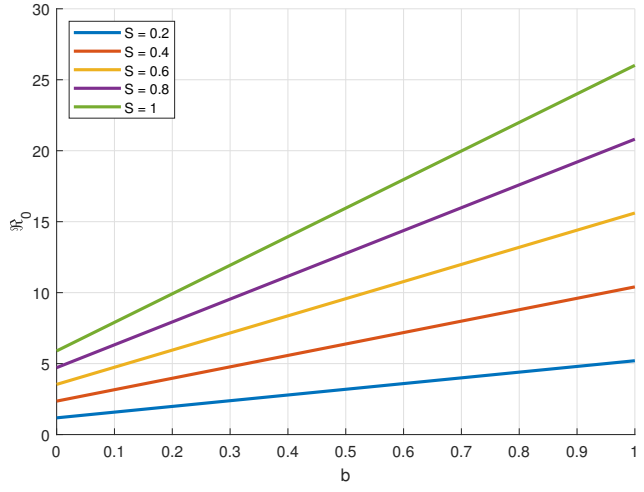

Figure 12: Combined effect of the rate at which the population becomes a victim of smoking and different values of S on $\mathfrak{R}_0$.

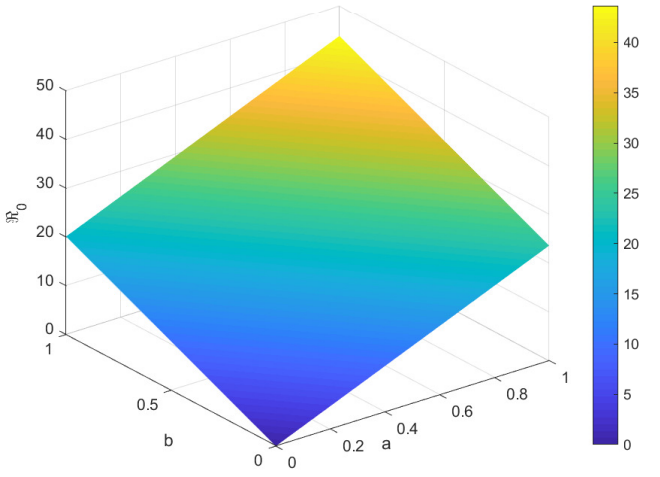

Figure 13: Combined effect of the rates b and a on $\mathfrak{R}_0$.

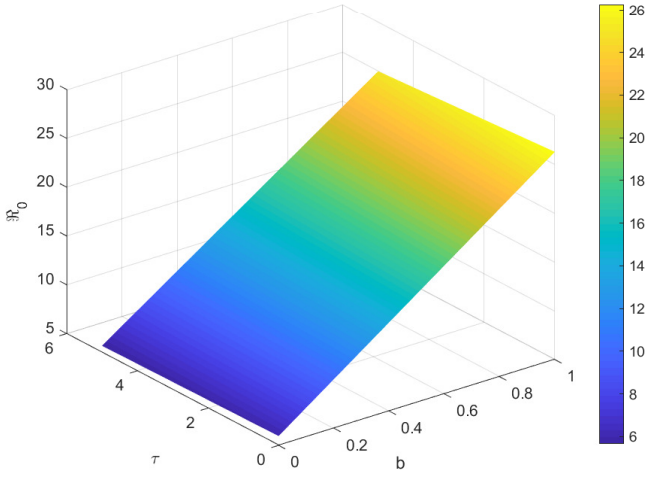

Figure 14: Combined effect of τ and b on $\mathfrak{R}_0$.

5. Conclusion

This research project constructs and examines a nonlinear mathematical model of LC dynamics with a time delay associated with smoking exposure and the evolution of smoking-related effects. The model is designed as a theoretical basis designed to get an idea of the qualitative behavior of the LC evolution and not a predictive tool. Biologically significant parameters are taken based on literature values to make the model acquire realistic dynamics of the disease. The delay acts through the interaction terms $S(t-\tau)M(t-\tau)$ and represents an exposure-related lag rather than a delayed treatment or immune-response mechanism. The results of this work offer qualitative information regarding the interaction between smoking and LC and the possible effect of the important parameters in the model on the course of the disease.

Mathematically, the model holds the crucial biological properties, such as, positivity and boundedness of the solutions, which implies that all the state variables have some meaning over time. The $\mathfrak{R}_0$ is calculated to describe the threshold dynamic of the system and both the DFE and EE stability analysis indicates that model parameters and delay effect have a strong influence in the dynamics of a system. Sensitivity analysis also determines the parameters that are the most sensitive in the course of disease, which gives insight into the factors that most strongly influence the model threshold quantity and LC-related compartmental dynamics.

Time delay plays an important role in the overall model dynamics. The displayed threshold expression shows that increasing the delay parameter decreases $\mathfrak{R}_0$ through the factor $e^{-m\tau}$ and influences the evolution of the smoking-related compartments. In this model, the delay represents the lag in smoking exposure and smoking-related effects rather than immune or treatment response. Numerical simulations further illustrate how the delay affects the long-term compartmental dynamics. In order to confirm the results of the analysis, numerical simulations are conducted with NSFD, Euler, and ($RK4$) methods.

The findings substantiate the fact that, although all the methods can capture the overall dynamics, the NSFD scheme is more stable and qualifies the properties of the continuous system, at least at large step sizes, than classical numerical methods.

In general, the presented research highlights that time delay in the model of LC should be used to better understand the dynamics of the disease in a more realistic way. The findings show that the parameters of the disease model and the delay effects have significant influence on the evolution of the disease process. Screening or treatment-control variables are not explicit in the present model but may be used as a foundation for future studies of screening or treatment-control variables. Furthermore, the proposed scheme can be a useful theoretical and computational framework for future studies of LC dynamics. This model could be further developed in future work with several delays, stochastic effects or fractional-order dynamics to model less complex biological behavior and uncertainties in the future development of LC.

Data availability

All data are available within the article.

Declaration of competing interest

The authors declare that there are no conflicts of interest.

Funding

This work was supported by a Universiti Sains Malaysia short-term grant (project number $R501 - LR - RND002 - 0000001136 - 0000$).

References

[1] I. B. Ekeanyanwu, P. Nwagor & I. George, "A binary stability and Monte Carlo simulation analysis of the simultaneous impact of smoking on the dynamics of lung cancer", Faculty of Natural and Applied Sciences Journal of Mathematical Modeling and Numerical Simulation **2** (2025) 132. https://www.fnasjournals.com/index.php/FNAS-JMNS/article/view/774.

[2] O. P. Loko, P. Nwagor & I. George, "A simulation study of predator–prey interaction model with changing climatic factors in an aquatic environment", Faculty of Natural and Applied Sciences Journal of Scientific Innovations **4** (2023) 211. https://www.fnasjournals.com/index.php/FNAS-JSI/article/view/136.

[3] N. Ilmayasinta, E. Anjarsari & M. W. Ahdi, "Optimal control for smoking epidemic model", 7th International Conference on Research, Implementation, and Education of Mathematics and Sciences (ICRIEMS 2020), Yogyakarta, Indonesia, 2021, pp. 323–328. https://doi.org/10.2991/assehr.k.210305.046.

[4] M. H. A. Biswas, L. T. Paiva & M. R. de Pinho, "A SEIR model for control of infectious diseases with constraints", Mathematical Biosciences and Engineering **11** (2014) 761. https://doi.org/10.3934/mbe.2014.11.761.

[5] D. Deb, S. Ghosh, S. Dalui, A. Dey & P. C. Sil, "Lung cancer in non-smokers: Molecular, immunological and potential therapeutic approaches", Indian Journal of Clinical Biochemistry (2026). https://doi.org/10.1007/s12291-026-01422-8.

[6] G. Dawson, "Cancer sourcebook, Health Reference Series", Journal of the National Medical Association **96** (2004) 1514.

[7] H.-U. Kauczor, L. Bonomo, M. Gaga, K. Nackaerts, N. Peled, M. Prokop, M. Remy-Jardin, O. von Stackelberg & J.-P. Sculier, "ESR/ERS white paper on lung cancer screening", European Radiology **25** (2015) 2519. https://doi.org/10.1007/s00330-015-3697-0.

[8] T. E. Roswarski, M. D. Murray & R. W. Proctor, "Framing, patient characteristics, and treatment selection in medical decision-making", in Human Interface and the Management of Information. Interacting in Information Environments, M. J. Smith & G. Salvendy (Eds.), Springer, Berlin, Heidelberg, Germany, 2007, pp. 315–322. https://doi.org/10.1007/978-3-540-76805-0_26.

[9] A. Besaratinia & G. P. Pfeifer, "Second-hand smoke and human lung cancer", The Lancet Oncology **9** (2008) 657. https://doi.org/10.1016/S1470-2045(08)70172-4.

[10] F. Brauer, "Infectious disease models with chronological age structure and epidemiological age structure", in Mathematical Approaches for Emerging and Reemerging Infectious Diseases: Models, Methods, and Theory, C. Castillo-Chavez, S. Blower, P. van den Driessche, D. Kirschner & A.-A. Yakubu (Eds.), Springer, New York, NY, USA, 2002, pp. 231–243. https://doi.org/10.1007/978-1-4613-0065-6_13.

[11] L. D. Johnston, P. M. O'Malley & J. G. Bachman, Smoking, Drinking, and Illicit Drug Use among American Secondary School Students, College Students, and Young Adults, 1975–1991, National Institute on Drug Abuse, U.S. Department of Health and Human Services, Rockville, MD, USA, 1992. NIH Publication No. 93-3480. Available online: https://monitoringthefuture.org/wp-content/uploads/2022/08/mtf-vol1_1991.pdf.

[12] G. Zaman, "Optimal campaign in the smoking dynamics", Computational and Mathematical Methods in Medicine **2011** (2011) 163834.https://doi.org/10.1155/2011/163834.

[13] G. ur Rahman, R. P. Agarwal & Q. Din, "Mathematical analysis of giving up smoking model via harmonic mean type incidence rate", Applied Mathematics and Computation **354** (2019) 128. https://doi.org/10.1016/j.amc.2019.01.053.

[14] G. M. S. Casagrande, M. de O. Silva, R. M. Reis & L. F. Leal, "Liquid biopsy for lung cancer: Up-to-date and perspectives for screening programs", International Journal of Molecular Sciences **24** (2023) 2505. https://doi.org/10.3390/ijms24032505.

[15] E. C. Farlow, K. Patel, S. Basu, B.-S. Lee, A. W. Kim, J. S. Coon, L. P. Faber, P. Bonomi, M. J. Liptay & J. A. Borgia, "Development of a multiplexed tumor-associated autoantibody-based blood test for the detection of non-small cell lung cancer", Clinical Cancer Research **16** (2010) 3452. https://doi.org/10.1158/1078-0432.CCR-09-3192.

[16] Trisilowati, "Stability analysis and optimal control of lung cancer growth model with education", IOP Conference Series: Materials Science and Engineering **546** (2019) 052081. https://doi.org/10.1088/1757-899X/546/5/052081.

[17] D. Gale, A. R. J. Lawson, K. Howarth, M. Madi, B. Durham, S. Smalley, J. Calaway, S. Blais, G. Jones, J. Clark, P. Dimitrov, M. Pugh, S. Woodhouse, M. Epstein, A. Fernandez-Gonzalez, A. S. Whale, J. F. Huggett, C. A. Foy, G. M. Jones, H. Raveh-Amit, K. Schmitt, A. Devonshire, E. Green, T. Forshew, V. Plagnol & N. Rosenfeld, "Development of a highly sensitive liquid biopsy platform to detect clinically relevant cancer mutations at low allele fractions in cell-free DNA", PLOS ONE **13** (2018) e0194630. https://doi.org/10.1371/journal.pone.0194630.

[18] V. Beljanski & J. Hiscott, "The use of oncolytic viruses to overcome lung cancer drug resistance", Current Opinion in Virology **2** (2012) 629. https://doi.org/10.1016/j.coviro.2012.07.006.

[19] R. Kanzaki, H. Chikaraishi, T. Tokunaga, H. Samejima, M. Kobayashi, T. Maniwa & J. Okami, "Treatment strategies and outcomes in patients with synchronous multiple primary malignancies involving lung cancer", International Journal of Clinical Oncology (2026). https://doi.org/10.1007/s10147-026-03098-9.

[20] A. Atangana & S. Igret Araz, "Modeling and forecasting the spread of COVID-19 with stochastic and deterministic approaches: Africa and Europe", Advances in Difference Equations **2021** (2021) 57. https://doi.org/10.1186/s13662-021-03213-2.

[21] H. J. de Koning, C. M. van der Aalst, P. A. de Jong, E. T. Scholten, K. Nackaerts, M. A. Heuvelmans, J.-W. J. Lammers, C. Weenink, U. Yousaf-Khan, N. Horeweg, S. van 't Westeinde, M. Prokop, W. P. Mali, F. A. A. Mohamed Hoesein, P. M. A. van Ooijen, J. G. J. V. Aerts, M. A. den Bakker, E. Thunnissen, J. Verschakelen, R. Vliegenthart, J. E. Walter, K.

ten Haaf, H. J. M. Groen & M. Oudkerk, "Reduced lung-cancer mortality with volume CT screening in a randomized trial", New England Journal of Medicine **382** (2020) 503. https://doi.org/10.1056/NEJMoa1911793.

[22] D. Jiang, Y. Wang, M. Liu, Q. Si, T. Wang, L. Pei, P. Wang, H. Ye, J. Shi, X. Wang, C. Song, K. Wang, L. Dai & J. Zhang, "A panel of autoantibodies against tumor-associated antigens in the early immunodiagnosis of lung cancer", Immunobiology **225** (2020) 151848. https://doi.org/10.1016/j.imbio.2019.09.007.

[23] Y. W. Kim, E. J. Park, K. I. Kwak, T. H. Yoon, H.-R. Kang, D.-H. Joo, Y. J. Lee, J. S. Park, J. H. Lee & C.-T. Lee, "Electronic cigarette use after smoking cessation and lung cancer risk", Nature Medicine **32** (2026) 2410. https://doi.org/10.1038/s41591-026-04469-5.

[24] A. Ahmad, M. Uzair Awan, S. Zeb, B. Ceesay, M. Rafiq, A. Kamran & A. Shaukat, "A delay mathematical model to examine control strategies of the coronavirus pandemic with an efficient approach", Advances in Differential Equations and Control Processes **32** (2025) 3703. https://doi.org/10.59400/adecp3703.

[25] J. H. Jung, A. Park & I. H. Jung, "Qualitative and sensitivity analysis of the effect of electronic cigarettes on smoking cessation", Computational and Mathematical Methods in Medicine **2018** (2018) 3738584. https://doi.org/10.1155/2018/3738584.

[26] A. Zeb, A. Bano, E. Alzahrani & G. Zaman, "Dynamical analysis of cigarette smoking model with a saturated incidence rate", AIP Advances **8** (2018) 045317. https://doi.org/10.1063/1.5028157.

[27] Q. Din, M. Ozair, T. Hussain & U. Saeed, "Qualitative behavior of a smoking model", Advances in Difference Equations **2016** (2016) 96. https://doi.org/10.1186/s13662-016-0830-6.

[28] Z. Zhang, R. Wei & W. Xia, "Dynamical analysis of a giving up smoking model with time delay", Advances in Difference Equations **2019** (2019) 505. https://doi.org/10.1186/s13662-019-2450-4.

[29] G. ur Rahman, R. P. Agarwal, L. Liu & A. Khan, "Threshold dynamics and optimal control of an age-structured giving up smoking model", Nonlinear Analysis: Real World Applications **43** (2018) 96. https://doi.org/10.1016/j.nonrwa.2018.02.006.

[30] S. Ucar, E. Ucar, N. Ozdemir & Z. Hammouch, "Mathematical analysis and numerical simulation for a smoking model with Atangana–Baleanu derivative", Chaos, Solitons & Fractals **118** (2019) 300. https://doi.org/10.1016/j.chaos.2018.12.003.

[31] A. Labzai, O. Balatif & M. Rachik, "Optimal control strategy for a discrete-time smoking model with specific saturated incidence rate", Discrete Dynamics in Nature and Society **2018** (2018) 5949303. https://doi.org/10.1155/2018/5949303.

[32] E. Alzahrani & A. Zeb, "Stability analysis and prevention strategies of tobacco smoking model", Boundary Value Problems **2020** (2020) 3. https://doi.org/10.1186/s13661-019-01315-1.

[33] P. Nwagor & P. S. Oghenrhoro, "SEIR model-based evaluation of the impact of smoking recruitment rates on lung cancer incidence and prevalence", Faculty of Natural and Applied Sciences Journal of Mathematical Modeling and Numerical Simulation **2** (2025) 113. https://doi.org/10.63561/jmns.v2i3.869.